# IONOSPHERIC ANALYSIS AND IONOSPHERIC MODELING

David C. Miller, et al

Arcon Corporation

Prepared for:

Air Force Cambridge Research Laboratories

July 1975

AFCRL-TR-75-0549



# IONOSPHERIC ANALYSIS AND IONOSPHERIC MODELING

David C. Miller
Joseph Gibbs

ARCON Corporation
Lakeside Office Park
Wakefield, Massachusetts 01880

July 1975

Scientific Report No. 2



AIR FORCE CAMBRIDGE RESEARCH LABORATORIES
AIR FORCE SYSTEMS COMMAND
UNITED STATES AIR FORCE
HANSCOM AFB, MASSACHUSETTS 01731

**DOCUMENT CONTROL DATA - R&D**

*(Security classification of title, body of abstract and indexing annotation must be entered when the overall report is classified)*

1. ORIGINATING ACTIVITY (Corporate author)
ARCON Corporation
Lakeside Office Park
Wakefield, Massachusetts 01880

2a. REPORT SECURITY CLASSIFICATION
Unclassified

2b. GROUP

3. REPORT TITLE

IONOSPHERIC ANALYSIS AND IONOSPHERIC MODELING

4. DESCRIPTIVE NOTES (Type of report and inclusive dates)
Scientific-Interim

5. AUTHOR(S) (First name, middle initial, last name)
David C. Miller
Joseph Gibbs

6. REPORT DATE
July 1975

7a. TOTAL NO. OF PAGES
87

7b. NO. OF REFS
10

8a. CONTRACT OR GRANT NO.
F19628-74-C-0070

b. PROJECT, TASK, WORK UNIT NOS.
5631-18-01

c. DOD ELEMENT
61102F

d. DOD SUBELEMENT
681310

9a. ORIGINATOR'S REPORT NUMBER(S)
Scientific Report No. 2

9b. OTHER REPORT NO(S) (Any other numbers that may be assigned this report)
AFCRL-TR-75-0549

10. DISTRIBUTION STATEMENT

Approved for public release; distribution unlimited.

11. SUPPLEMENTARY NOTES

Tech Other

12. SPONSORING MILITARY ACTIVITY
Air Force Cambridge Research Laboratories
Hanscom Air Force Base, Mass. 01731
Contract Monitor: Charles M. Rush/LII

13. ABSTRACT

In this report, we describe several investigations performed towards improving our knowledge of the ionosphere and our ability to communicate through the ionosphere. A global ionospheric model of the ionosphere was developed which allows for the incorporation of hourly observations of ionospheric parameters. A polar ionospheric model for foF2 was developed which contains corrections to a median model which are characteristic of the polar region. Improvements in ionospheric ray tracing techniques are described including the development of a homing procedure.



DD FORM 1 NOV 65 1473

Unclassified

Security Classification

| 14. KEY WORDS | LINK A | | LINK B | | LINK C | |
|---|---|---|---|---|---|---|
| | ROLE | WT | ROLE | WT | ROLE | WT |
| Ionospheric Modeling | | | | | | |
| Ionospheric Forecasting | | | | | | |
| Ionospheric Ray Tracing | | | | | | |
| Polar Ionosphere | | | | | | |

2.

Security Classification

TABLE OF CONTENTS

# I. GLOBAL IONOSPHERIC MODELING

The requirements of more accurate methods for assessing HF radio propagation and detection conditions has intensified the efforts to produce better models of the ionosphere. We report here some results of our continued effort in this area. In a previous report [1] we described some techniques we had developed and some computer programs written toward the construction of a three dimensional ionospheric model. This model attempted to reduce some of the deficiencies associated with models based upon our current knowledge of the physical and chemical processes occurring in the ionosphere by the inclusion of some observations of ionospheric parameters.

We have concentrated our effort to predicting and specifying the most variable ionospheric region—the F2 region. Previous work [2] has indicated that the daily variability of the critical frequency of the F2 region, foF2, is two to three times that of the critical frequency of the lower ionospheric regions. The techniques we employ for modeling foF2 are also used in modeling hmF2, the maximum height of the F2 region but have been developed only from studies of the spatial and temporal variability of foF2. Studies using ray tracing techniques have shown the inaccuracies in specifying foF2 along a ray path are responsible in most part for errors in predicting HF propagation conditions.

It is shown in reference 1 that our approach to modeling foF2 consists in updating or modifying a first guess ionosphere with observations of foF2 both at irregular locations and random hours. These observations over the globe are extended and extrapolated over larger regions using a synoptic mapping technique similar to that used by meteorologists for obtaining weather maps when only sparse observations are available. The model and method for determining the vertical electron density distribution

given foF2 and hm.F2 has not been changed and will not be described here. We have used several sets of ionospheric data in establishing the techniques and in verifying the accuracy of the maps that were generated.

A. The 1958 IGY measurements of foF2 available from a network of 157 vertical incidence ionosondes spread over the entire globe.

B. Measurements of foF2 from a set of 36 vertical incidence ionosondes over Europe and Asia during the years 1960, 1962, 1966 and 1968. Data was also available from the same network for four months during 1964.

These data span a full solar cycle and allowed one to test the modeling procedures over periods of both high and low solar activity.

## IONOSPHERIC GRID MODELING

The determination of foF2 on a global scale consists of two separate steps which can be modified independent of each other. The first part of the modeling procedure consists of making an initial estimate of foF2 at arbitrary locations and times over a region of interest. The sparseness and nonuniformity of the available data requires that this estimate contain most of the general physical features of the ionosphere. We have experimented with several first-guess ionospheres and in particular problems have used more than one in producing maps for series of hourly analysis. The most general accepted predictions of foF2 are the monthly median maps due to Jones and Gallet [3]. Their model describes foF2 as a spherical harmonic expansion in terms of $\phi$. the geographic longitude, $\lambda$ the geographic latitude and T. the universal time. The diurnal variation has been separated from the spatial variation according to

$$\text{foF2}(\phi, \lambda, T) = \sum_{k=0}^{76} D_k(T)\, G_k(\phi, \lambda). \qquad (1)$$

The coefficients of the expansion have been related to the 12-month running mean Zurich sunspot number so that the model predicts median ionospheric conditions. The monthly median model is used whenever no other analysis is available. When ionospheric maps are to be made in hourly increments, we have used as the first-guess ionosphere updated maps of the previous hour. The map is rotated 15° of geographic longitude to the west as a station displaced by 15° to the west would be expected to observe a similar ionosphere one hour later.

Most applications of our predictions require that the ionosphere be specified on a uniform grid coordinate system. The output of our analysis

is always given in geographic coordinates with equal spacings in latitude and longitude. We have found that a grid spacing of 15° in longitude and 10° in latitude allows us to preserve most of the important ionospheric features of the F2 region. This spacing gives us a grid which is 25 X 19. In some areas, most notable the high latitude trough and the region of the equitorial anomaly a smaller spacing in latitude may be necessary.

In our original work, our modeling procedure was also carried out in a uniform grid in geographic coordinates. Since many features in the F2 region tend to be aligned along lines of constant geomagnetic latitude, we have chosen values of the grid locations (the grid is still 25 X 19) to spaced 15° apart in geographic longitude and 10° apart in geomagnetic latitude. Although this is not an orthogonal coordinate system, it has no effect on the modeling procedure.

The first guess ionosphere for a given universal time is used to determine the value of foF2 at each of the grid points $\phi_{gi}$, $\lambda_{mj}$ and at the location of each observation $\phi_{gl}$, $\lambda_{ml}$ where $\phi_g$ is geographic longitude and $\lambda_m$ is dipole geomagnetic latitude. Using this, we calculate the deviation between first guess and the observation:

$$D_\ell \equiv FG(\phi_\ell, \lambda_\ell, T) - OBS_\ell \qquad (2)$$

where we have suppressed the indices denoting our mixed coordinate system. We also calculate for the N stations reporting the average residual $D_R$

$$D_R = \frac{1}{N} \sum_{\ell=1}^{N} D_\ell \qquad (3)$$

and the average square residual $\overline{D_R^2}$,

$$\overline{D_R^2} = \frac{1}{N} \sum_{\ell=1}^{N} D_\ell^2 \tag{4}$$

The influence of the individual deviations $D_\ell$ is extended to the points on the grid by employing a weighting scheme. The corrections to the first guess field at a grid point for an individual observation can be written as

$$D_{ij\ell} = W^{(1)}_{i\ell} \; W^{(2)}_{j\ell} \; D_\ell \tag{5}$$

where the exact form of the W's is given in reference (1). The weighting factors depend upon north-south and east-west geographic separations between stations and grid points. The total correction to each grid point is:

$$D_{ij} = \frac{\sum_{\ell=1}^{N} W^{(1)}_{i\ell} \; W^{(2)}_{j\ell} \; D_{ij\ell}}{\sum_{\ell=1}^{N} W^{(1)}_{i\ell} \; W^{2}_{j\ell}} \tag{6}$$

The updated grid of values of foF2, $U_{ij}$ is then computed using these corrections and the first guess field using

$$U_{ij} = FG_{ij} - D_{ij} \tag{7}$$

The updating procedure is carried out a total of four times with the updated field $U_{ij}$ becoming a new first guess field, $FG_{ij}$, for the next iteration. After each iteration, a bilinear interpolation is performed between the four surrounding grid points of each observation to provide a new residual. The magnitude of the weighting factors is reduced by a factor of two after each iteration, but is not allowed to decrease below a minimum value. If we define

$$W_{ij\ell} = W^{(1)}_{i\ell}\, W^{(2)}_{j\ell} \tag{8}$$

then the grid correction $D_{ij}$ can be written as

$$D_{ij} = \frac{\sum_{\ell=1}^{N} W_{ij\ell}\, D_\ell}{\sum_{\ell=1}^{N} W_{ij\ell}} \tag{9}$$

In order to examine the behavior of this correction, we separate out that contribute which results when only the minimum weight $W_o$ is used.

$$D_{ij} = \frac{\sum_{\ell=1}^{M} W_{ij\ell}\, D_\ell \;+\; W_o \sum_{\ell=M+1}^{N} D_\ell}{\sum_{\ell=1}^{M} W_{ij\ell} \;+\; (N-M)\, W_o} \tag{10}$$

In this expression, M observations contribute with a weight $W_{ij\ell} > W_o$, and N—M contribute with weight $W_o$. For a given local time and season, $W_{ij\ell}$ is dependent upon the distance between grid points and observations and characteristically goes to zero between 2,500 and 7,500 kilometers for the first iteration and between 300 and 900 kilometers for the fourth iteration. An indication of the size of the correction produced by $W_o$ not being zero is given in regions where N=0, that is no nearby observations. Here $D_{ij} = D_R$ the average residual for the iteration. In almost all cases $|D_R| < 0.1$ Mhz. after the first iteration. In addition to providing an average correction to the entire globe, the use of a non zero weight insures a smooth behavior of $D_{ij}$ at the boundary of regions where observations do not exist. If N=1 and $W_o$=0 then $D_{ij} = D_\ell$ independent of separation between grid point and obser-

vation. This condition can produce a large correction for distances up to 7,500 kilometers.

We have incorporated into the analysis program the capability of calculating the individual deviations, and the average, $D_R$, and rms deviation $\sqrt{\overline{D_R^2}}$ for groups of verifying stations not used to update the first-guess map. These parameters provided an indication of the validity of the analysis at points away from the observations used in the analysis. We present here an example of such a study in which the 157 stations of 1958 were randomly divided into two sets of stations. In Table I-1, the results are shown for four hours during January 24, 1958. The number of actual observations available in each of the time periods is comparable for both station groups. Table II-2a presents a comparison between the individual observations and the first-guess model using the ITS coefficients and the final updated map using the modeling stations for UT=1800 hours, January 24, 1958. Table II-2B presents the same information for the verification stations.

We can see from Table 1 that when observations are available on a global basis the residuals at both sets of stations are independent of time. Studies of the 1958 data [4] have shown that the residuals, $D_R$ and $\sqrt{\overline{D_R^2}}$ determined from the modeling stations are approximately the same when the number of stations was in the range of 25-100. It can be stated that in regions where data are available, the modeling procedure yields maps that are a good representation of the observations. Figure I-1 is a contour plot of foF2 values on a cylindrical equidistant global map for the data given in Table I-2a. In all analysis, the general shape of the gradients seen on the maps that used daily hourly data were similar to the monthly median for the same hour. For the range of numbers of observations used in the analysis, the general shape of the median map was retained and the values of map contours were raised or lowered in accordance with the observations.

RESULTS OF MODELING AND VERIFICATION ANALYSIS FOR JANUARY 24, 1958

| Universal Time | | 000 | | 600 | | 1200 | | 1800 | |
|---|---|---|---|---|---|---|---|---|---|
| | | Modeling | Verification | Modeling | Verification | Modeling | Verification | Modeling | Verification |
| Number of Stations | | 43 | 42 | 52 | 44 | 46 | 40 | 48 | 40 |
| First Guess | $D_R$ | 0.49 | 0.24 | 0.72 | 0.84 | 0.37 | 1.09 | 0.42 | 0.72 |
| | $\sqrt{D_R^2}$ | 2.56 | 2.34 | 2.31 | 1.89 | 2.52 | 2.14 | 2.15 | 2.10 |
| Final Map (4th Iteration) | $D_R$ | -0.09 | -0.09 | -0.07 | 0.18 | -0.06 | 0.56 | 0.04 | 0.25 |
| | $\sqrt{D_R^2}$ | 0.78 | 1.58 | 0.62 | 1.02 | 0.60 | 1.67 | 0.72 | 1.28 |

TABLE I-1

TABLE I-2a

MEASURED DATA JAN 24 18.0 GMT SSN=137. XKP= 2. WO= 181.

MODELING STATIONS

MODEL IS ITS COEFFICIENTS

| DAY | LT | CODE | NAME | LONG | LAT | ITS MODEL | MEAS | RESIDUAL | UPDATED MODEL | UPDATED RESIDUAL |
|---|---|---|---|---|---|---|---|---|---|---|
| 1 | 24 | 14 | J82 | -62.000 | 82.000 | 5.418 | 6.800 | -1.382 | 6.512 | -.288 |
| 2 | 24 | 15 | J47 | -52.000 | 47.000 | 10.358 | 14.500 | -4.142 | 13.751 | -.749 |
| 3 | 24 | 14 | J70 | -68.000 | 70.000 | 7.101 | 11.000 | -3.899 | 10.310 | -.690 |
| 4 | 24 | 17 | A84 | -21.000 | 64.000 | 5.693 | 5.200 | .493 | 6.724 | 1.524 |
| 5 | 24 | 14 | J40 | -74.000 | 40.000 | 12.080 | 14.000 | -1.920 | 14.009 | .009 |
| 6 | 24 | 11 | 832 | -106.000 | 32.000 | 11.694 | 14.600 | -2.906 | 14.576 | -.024 |
| 7 | 24 | 14 | J16 | -67.000 | 18.000 | 11.398 | 12.200 | -.802 | 12.658 | .458 |
| 8 | 24 | 18 | 241 | 12.000 | 41.000 | 6.685 | 9.800 | -3.115 | 9.766 | .066 |
| 9 | 24 | 20 | 144 | 34.000 | 44.000 | 4.339 | 5.000 | -.661 | 6.506 | 1.506 |
| 10 | 25 | 2 | 416 | 120.000 | 16.000 | 7.619 | 7.700 | -.081 | 7.523 | -.177 |
| 11 | 24 | 21 | 237 | 58.000 | 37.000 | 3.314 | 5.500 | -2.186 | 5.537 | .037 |
| 12 | 24 | 23 | 343 | 76.000 | 43.000 | 2.751 | 5.200 | -2.449 | 5.081 | -.119 |
| 13 | 25 | 2 | 424 | 121.000 | 25.000 | 5.423 | 5.600 | -.177 | 5.656 | .056 |
| 14 | 25 | 2 | 431 | 130.000 | 31.000 | 4.279 | 4.300 | -.021 | 4.364 | .064 |
| 15 | 25 | 3 | 539 | 140.000 | 39.000 | 3.224 | 4.200 | -.976 | 4.227 | .027 |
| 16 | 24 | 23 | 313 | MADRAS | 80.000 | 13.000 | 10.589 | 10.800 | -.211 | 10.491 | -.309 |
| 17 | 24 | 23 | 311 | TRIJCHIRAPPALLI | 78.000 | 10.000 | 9.746 | 10.200 | -.454 | 10.266 | .066 |
| 18 | 24 | 19 | 10K | LWIRO | 28.000 | -2.000 | 11.733 | 11.800 | -.067 | 11.961 | .181 |
| 19 | 24 | 9 | 71P | TAHITI | -149.000 | -17.000 | 10.446 | 12.600 | -2.154 | 12.448 | -.152 |
| 20 | 24 | 8 | 770 | LITTLE AMERICA | -162.000 | -78.000 | 5.862 | 6.300 | -.438 | 6.298 | -.002 |
| 21 | 24 | 15 | J5J | PORT STANLEY | -57.000 | -51.000 | 9.556 | 9.800 | -.244 | 9.800 | .000 |
| 22 | 24 | 14 | J6M | ARGENTINE ISL. | -64.000 | -65.000 | 7.312 | 7.600 | -.288 | 7.623 | .023 |
| 23 | 24 | 19 | 11J | ELIZABETHVILLE | 27.000 | -11.000 | 10.890 | 12.500 | -1.610 | 12.394 | -.106 |
| 24 | 24 | 22 | 248 | KERGUELEN | 70.000 | -49.000 | 6.083 | 4.300 | 1.783 | 4.363 | .063 |
| 25 | 25 | 4 | 52P | BRISBANE | 152.000 | -27.000 | 7.338 | 6.700 | .638 | 6.751 | .051 |
| 26 | 25 | 3 | 54K | HOBART | 147.000 | -42.000 | 5.300 | 5.500 | -.200 | 5.470 | -.030 |
| 27 | 24 | 14 | J05 | BOGOTA | -74.000 | 4.000 | 13.043 | 14.200 | -1.157 | 14.489 | .289 |
| 28 | 24 | 13 | 909 | PANAMA | -79.000 | 9.000 | 12.400 | 14.400 | -2.000 | 14.190 | -.210 |
| 29 | 25 | 0 | 361 | SINGAPORE | 103.000 | 1.000 | 9.298 | 10.000 | -.702 | 9.995 | -.005 |
| 30 | 24 | 12 | 354 | BAKER LAKE | -96.000 | 64.000 | 8.108 | 9.700 | -1.592 | 10.267 | .567 |
| 31 | 24 | 12 | 949 | WINNIPEG | -94.000 | 49.000 | 11.090 | 13.500 | -2.410 | 13.470 | -.030 |
| 32 | 24 | 13 | 980 | EUREKA | -85.000 | 80.000 | 5.532 | 5.200 | .332 | 5.483 | .283 |
| 33 | 24 | 16 | 546 | POITIERS | 0.000 | 46.000 | 6.523 | 9.000 | -2.477 | 9.660 | .660 |
| 34 | 24 | 15 | 549 | DOURBES | 4.000 | 50.000 | 5.588 | 8.500 | -2.912 | 9.058 | .558 |
| 35 | 24 | 18 | 053 | DE BILT | 5.000 | 52.000 | 5.221 | 8.500 | -3.279 | 8.620 | .120 |
| 36 | 24 | 18 | 056 | LINDAU | 10.000 | 51.000 | 5.022 | 10.200 | -5.178 | 9.102 | -1.098 |
| 37 | 24 | 18 | 755 | JULIUSRUH | 13.000 | 54.000 | 4.423 | 9.800 | -5.377 | 8.172 | -1.628 |
| 38 | 24 | 17 | 158 | UPPSALA | 17.000 | 59.000 | 3.695 | 6.100 | -2.405 | 6.139 | .039 |
| 39 | 24 | 19 | 167 | KIRUNA | 20.000 | 67.000 | 3.276 | 6.300 | -3.024 | 5.221 | -1.079 |
| 40 | 24 | 19 | 165 | LULEA | 22.000 | 65.000 | 3.223 | 2.100 | 1.123 | 5.321 | 3.221 |
| 41 | 24 | 19 | 159 | NURMIJARVI | 24.000 | 60.000 | 3.319 | 5.900 | -2.581 | 5.420 | -.480 |
| 42 | 24 | 20 | 165 | MURMANSK | 33.000 | 69.000 | 3.086 | 5.500 | -2.414 | 5.247 | -.253 |
| 43 | 24 | 20 | 149 | ROSTOV | 39.000 | 47.000 | 3.662 | 6.700 | -3.038 | 6.018 | -.682 |
| 44 | 24 | 22 | 256 | SVERDLOVSK | 61.000 | 56.000 | 2.880 | 4.400 | -1.520 | 4.623 | .223 |
| 45 | 25 | 2 | 462 | YAKUTSK | 129.000 | 62.000 | 3.578 | 2.800 | .778 | 3.121 | .321 |
| 46 | 25 | 3 | 947 | YUZHNO SAKHALINSK | 143.000 | 47.000 | 2.681 | 5.000 | -2.319 | 4.459 | -.541 |
| 47 | 24 | 9 | 761 | ANCHORAGE | -149.000 | 61.000 | 4.785 | 7.800 | -3.015 | 7.793 | -.007 |
| 48 | 24 | 11 | 855 | MEANOOK | -113.000 | 54.000 | 9.067 | 11.500 | -2.433 | 11.355 | -.145 |

NUMBER OF STATIONS IS 4 AVERAGE RESIDUAL FOF2 = -1.584 AVERAGE RESIDUAL FOF2 SQUARED = 4.942
(ITS MODEL)

NUMBER OF STATIONS IS 4 AVERAGE RESIDUAL FOF2 = .033 AVERAGE RESIDUAL FOF2 SQUARED = .501
(UPDATED MAP ANALYSIS)

TABLE I-2b

VERIFICATION STATIONS

| | | | | | | | | | | | |
|---|---|---|---|---|---|---|---|---|---|---|---|
| 49 | 24 | 15 | J61 | NARSSARSSUAQ | -45.000 | 61.000 | 7.870 | 9.200 | -1.330 | 10.333 | 1.133 |
| 50 | 24 | 13 | 945 | OTTAWA | -75.000 | 45.000 | 11.757 | 14.200 | -2.443 | 13.959 | -.241 |
| 51 | 24 | 13 | 938 | WASHINGTON | -77.000 | 38.000 | 12.234 | 14.000 | -1.766 | 13.967 | -.033 |
| 52 | 24 | 10 | 837 | SAN FRANCISCO | -122.000 | 37.000 | 10.688 | 13.800 | -3.112 | 13.437 | -.363 |
| 53 | 24 | 13 | 926 | GRAND BAHAMA | -78.000 | 26.000 | 12.027 | 13.200 | -1.173 | 13.487 | .287 |
| 54 | 24 | 8 | 728 | MAUI | -156.000 | 20.000 | 9.364 | 10.400 | -1.036 | 9.337 | -1.063 |
| 55 | 24 | 18 | 040 | TORTOSA | 0.000 | 40.000 | 7.686 | 9.300 | -1.614 | 10.924 | 1.624 |
| 56 | 24 | 22 | 219 | BOMBAY | 72.000 | 19.000 | 11.362 | 13.400 | -2.038 | 11.538 | -1.862 |
| 57 | 24 | 23 | 328 | DELHI | 77.000 | 28.000 | 4.835 | 8.600 | -3.765 | 6.757 | -1.843 |
| 58 | 25 | 2 | 426 | OKINAWA | 127.000 | 26.000 | 5.162 | 5.300 | -.138 | 5.250 | -.050 |
| 59 | 25 | 3 | 535 | TOKYO | 139.000 | 35.000 | 3.650 | 3.900 | -.250 | 4.315 | .415 |
| 60 | 25 | 3 | 545 | WAKKANAI | 141.000 | 45.000 | 2.816 | 4.700 | -1.884 | 4.406 | -.294 |
| 61 | 24 | 23 | 310 | KODAIKANAL | 77.000 | 10.000 | 9.766 | 9.800 | -.034 | 10.291 | .491 |
| 62 | 24 | 13 | 90M | TALARA | -81.000 | -4.000 | 13.488 | 13.000 | .488 | 14.499 | 1.499 |
| 63 | 24 | 8 | 72J | RAROTONGA | -159.000 | -21.000 | 9.733 | 12.700 | -2.967 | 11.450 | -1.250 |
| 64 | 24 | 13 | 90R | CHIMBOTE | -79.000 | -9.000 | 12.307 | 11.600 | .707 | 13.577 | 1.977 |
| 65 | 24 | 16 | A7P | ELLSWORTH | -41.000 | -77.000 | 6.440 | 7.000 | -.560 | 6.746 | -.254 |
| 66 | 24 | 15 | J2L | SAO PAULO | -46.000 | -23.000 | 13.131 | 13.800 | -.669 | 13.815 | .015 |
| 67 | 24 | 19 | 11? | TSUMEB | 17.000 | -19.000 | 10.261 | 10.800 | -.539 | 11.687 | .887 |
| 68 | 24 | 19 | 1?? | CAPETOWN | 18.000 | -34.000 | 8.718 | 9.800 | -1.082 | 9.011 | -.789 |
| 69 | 25 | 3 | 53N | CANBERRA | 149.000 | -35.000 | 6.174 | 7.000 | -.826 | 6.027 | -.973 |
| 70 | 25 | 5 | 64L | GODLEY HEAD | 172.000 | -43.000 | 6.266 | 6.400 | -.134 | 6.266 | -.134 |
| 71 | 25 | 5 | 67K | CAPE HALLET | 170.000 | -72.000 | 5.542 | 6.700 | -1.158 | 5.910 | -.790 |
| 72 | 25 | 5 | 67Q | SCOTT BASE | 166.000 | -77.000 | 5.640 | 7.100 | -1.460 | 6.050 | -1.050 |
| 73 | 24 | 18 | 007 | IBADAN | 3.000 | 7.000 | 10.511 | 11.300 | -.789 | 11.353 | .053 |
| 74 | 24 | 23 | 308 | TRIVANDRUM | 77.000 | 8.000 | 9.750 | 9.500 | .250 | 10.619 | 1.119 |
| 75 | 24 | 12 | 958 | CHURCHILL | -94.000 | 58.000 | 9.478 | 12.100 | -2.622 | 11.587 | -.513 |
| 76 | 24 | 12 | 974 | RESOLUTE BAY | -94.000 | 74.000 | 6.175 | 6.000 | .175 | 7.733 | 1.733 |
| 77 | 24 | 18 | 056 | INVERNESS | -4.000 | 57.000 | 5.213 | 8.200 | -2.987 | 7.686 | -.514 |
| 78 | 24 | 18 | 051 | SLOUGH | 0.000 | 51.000 | 5.721 | 9.700 | -3.979 | 8.635 | -1.065 |
| 79 | 24 | 18 | 452 | CHITA | 5.000 | 52.000 | 5.221 | 12.500 | -7.279 | 8.620 | -3.880 |
| 80 | 24 | 18 | 048 | FREIBURG | 7.000 | 48.000 | 5.698 | 8.500 | -2.802 | 9.456 | .956 |
| 81 | 24 | 19 | 164 | LYCKSELE | 18.000 | 64.000 | 3.382 | 2.300 | 1.082 | 5.427 | 3.127 |
| 82 | 24 | 19 | 169 | TROMSO | 19.000 | 69.000 | 3.332 | 3.300 | .032 | 5.079 | 1.779 |
| 83 | 24 | 20 | 160 | LENINGRAD | 30.000 | 60.000 | 3.113 | 4.300 | -1.187 | 5.112 | .812 |
| 84 | 24 | 20 | 155 | MOSCOW | 37.000 | 55.000 | 3.145 | 4.700 | -1.555 | 5.744 | 1.044 |
| 85 | 24 | 22 | 266 | SALAKHARD | 66.000 | 66.000 | 3.261 | 5.100 | -1.839 | 5.233 | -.067 |
| 86 | 24 | 7 | 651 | ADAK | -176.000 | 51.000 | 2.974 | 4.300 | -1.326 | 5.334 | 1.034 |
| 87 | 24 | 8 | 771 | BARROW | -156.000 | 71.000 | 4.007 | 4.200 | -.193 | 6.072 | 1.872 |
| 88 | 24 | 11 | 862 | YELLOWKNIFE | -114.000 | 62.000 | 7.531 | 10.100 | -2.569 | 9.616 | -.484 |

NUMBER OF STATIONS IS 40 AVERAGE RESIDUAL FOF2 = -1.409 AVERAGE RESIDUAL FOF2 SQUARED = 4.336
(ITS MODEL)

NUMBER OF STATIONS IS 4. AVERAGE RESIDUAL FOF2 = .109 AVERAGE RESIDUAL FOF2 SQUARED = 1.649
(UPDATED MAP ANALYSIS)

Contours of foF2 Values: Updated Ionosphere

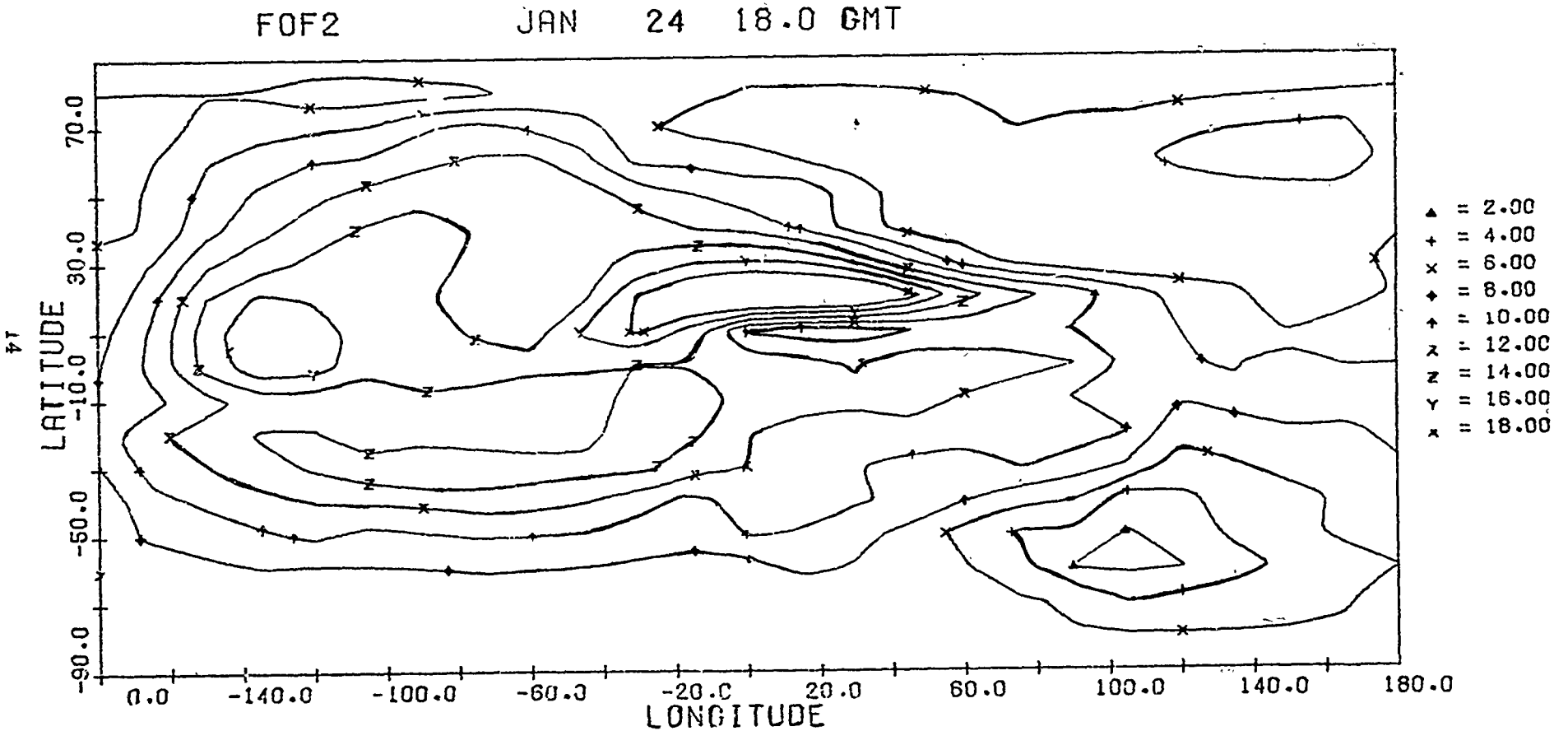


Figure I-1

For the data of Table I-2, the average improvement in the rms residual for the set of modeling stations is 1.8Mhz. and for the set of verification stations it is 0.7Mhz. A more detailed study of the improvement in the daily specification of foF2 as compared with the median ionospheric structure is presented in reference 4. In this study, the improvement resulting from the analysis of daily hourly data is given as a function of various latitudinal regions and seasons.

## IONOSPHERIC PREDICTIONS

The first guess foF2 field each hour can be considered the prediction for that hour. The advantage of the ITS monthly median model is that it can be used as a prediction for arbitrary time periods. The chief disadvantage in using the median prediction is that it does not reflect the day-to-day variability of the F2 region. The updated maps based upon our modeling procedure represent a more accurate description of the F2 layer for an hour in which observations of foF2 are available. We have studied two methods by which these analysis of past data may be used to make a prediction for future ionospheric behavior.

The first method, which we mentioned when describing the first guess ionosphere is to use the updated analysis made one hour in advance of the desired prediction. The prediction for foF2 is obtained from the grid values by using

$$foF2(\phi_{gi},\ \lambda_{mj},\ T+1) = foF2(\phi_{gi+1},\ \lambda_{mj}, T) \qquad (11)$$

where the variables have already been described. Since the modeling procedure is based upon the calculation of angular separations between grid points and observation locations in an orthogonal coordinate system, we must perform transformations between this mixed coordinate system and geographic coordinates. Both coordinate systems are shown in the following figure.

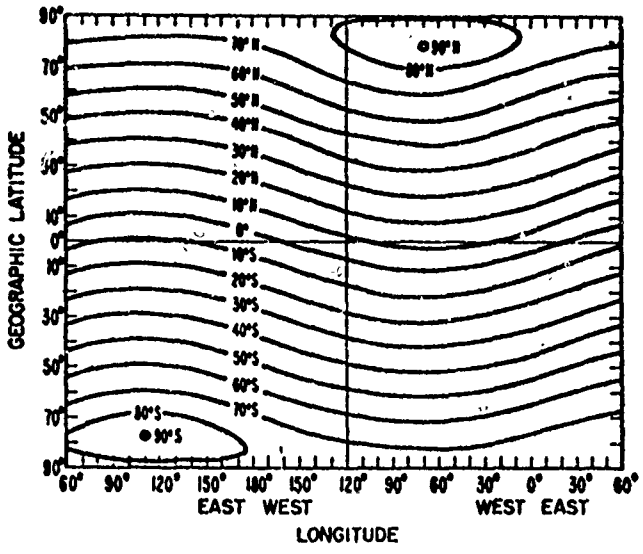


*World map of magnetic dipole latitude.*

Figure I-2

The grid used in expression (11) is specified by equal spacing in magnetic dipole latitude, $\lambda_{mj}$. To carry out all transformations, we store the grid of values of geographic latitude corresponding to the regularly spaced coordinates, $\phi_{gi}$, $\lambda_{mj}$. That is

$$\lambda_{gij} = H(\phi_{gi}, \lambda_{mj}) \tag{12}$$

This grid is determined using the equations which specify the transformation of one spherical coordinate system to another by a rotation matrix. In our case, we use the equation

$$\sin \lambda_{mj} = (R_{13} \cos \phi_{gi} + R_{23} \sin \phi_{gi}) \cos \lambda_{gij} + R_{33} \sin \lambda_{gij} \qquad (13)$$

where

$$R_{13} = \cos 78.3^{\circ} \cos 291.0^{\circ}$$

$$R_{23} = \cos 78.3^{\circ} \sin 291.0^{\circ}$$

$$R_{33} = \sin 78.3^{\circ}$$

For each grid value $\phi_{gi}$, $\lambda_{mj}$, we choose one of the two solutions of equation (13) for $\lambda_{gij}$. As can be seen from the world map of figure 2, not all values of $\phi_{gi}$, $\lambda_{mj}$ lead to a corresponding $\lambda$gij. The results for the 25 X 19 grid of equal spacing of $\phi_{gi}$, $\lambda_{mj}$ is given in Table I-3, where a value of 999.0 indicates that a coordinate does not yield a transformation. The modeling procedure is carried out in the regular mixed coordinate system $\phi$gi, $\lambda$mj with the weights of observations at the grid points given in terms of the angular separations $(\phi_{gi} - \phi^{obs}_{g\ell})$ and $(\lambda_{gij} - \lambda^{obs}_{g\ell})$. In order to determine foF2 at arbitrary locations, a linear interpolation in magnetic dipole latitude is performed on the great circle of constant geographic latitude. These interpolations are carried out after each iteration step in order to calculate the new residuals at station locations and at the end of the analysis to determine a final grid map in geographic coordinates.

Several tests were performed to determine the differences between this modeling procedure and one in which only geographic coordinates are used. If no observations are used, the only possible change in the final map must be due to the successive interpolations performed on the median ionosphere between the two coordinate systems. This was observed to be of the order

Transformation Grid H ($\phi_{gi}$, $\lambda_{mj}$) 24 X 19

| | | | | | | | | | | | | | | | | | | | | | | | |
|---|---|---|---|---|---|---|---|---|---|---|---|---|---|---|---|---|---|---|---|---|---|---|---|
| 1 | 999. | 999. | 999. | 999. | 999. | 999. | 999. | 999. | 999. | 999. | 999. | 999. | 999. | 999. | 999. | 999. | 999. | 999. | 999. | 999. | 999. | 999. | 999. |
| 2 | 999. | 999. | 999. | 999. | 78. | 73. | 70. | 68. | 69. | 70. | 74. | 80. | 999. | 999. | 999. | 999. | 999. | 999. | 999. | 999. | 999. | 999. | 999. |
| 3 | 77. | 75. | 72. | 68. | 65. | 62. | 59. | 58. | 59. | 60. | 62. | 65. | 69. | 72. | 75. | 78. | 80. | 81. | 81. | 82. | 82. | 81. | 80. | 79. |
| 4 | 66. | 63. | 60. | 57. | 54. | 51. | 49. | 48. | 48. | 50. | 52. | 54. | 58. | 61. | 64. | 67. | 69. | 70. | 71. | 72. | 72. | 71. | 70. | 68. |
| 5 | 56. | 53. | 50. | 46. | 43. | 41. | 39. | 38. | 38. | 40. | 41. | 44. | 47. | 50. | 53. | 56. | 58. | 60. | 61. | 62. | 62. | 61. | 60. | 58. |
| 6 | 45. | 42. | 39. | 36. | 33. | 31. | 29. | 28. | 28. | 29. | 31. | 34. | 37. | 40. | 43. | 46. | 48. | 50. | 51. | 52. | 52. | 51. | 50. | 48. |
| 7 | 35. | 32. | 29. | 26. | 23. | 21. | 19. | 18. | 18. | 19. | 21. | 24. | 26. | 29. | 33. | 35. | 38. | 40. | 41. | 42. | 42. | 41. | 39. | 37. |
| 8 | 25. | 22. | 19. | 16. | 13. | 11. | 9. | 8. | 8. | 9. | 11. | 13. | 16. | 19. | 22. | 25. | 28. | 30. | 31. | 32. | 32. | 31. | 29. | 27. |
| 9 | 14. | 11. | 8. | 5. | 3. | 1. | -1. | -2. | -2. | -1. | 1. | 3. | 6. | 9. | 12. | 15. | 18. | 20. | 21. | 22. | 22. | 21. | 19. | 17. |
| 10 | +4. | +1. | -2. | -5. | -7. | -10. | -11. | -12. | -12. | -11. | -9. | -7. | -4. | -1. | +2. | -5. | +7. | +10. | +11. | +12. | +12. | +11. | +9. | +7. |
| 11 | -6. | -9. | -12. | -15. | -18. | -20. | -21. | -22. | -22. | -21. | -19. | -17. | -14. | -11. | -8. | -5. | -3. | -1. | +1. | +2. | +2. | +1. | -1. | -3. |
| 12 | -16. | -19. | -22. | -25. | -28. | -30. | -31. | -32. | -32. | -31. | -29. | -27. | -25. | -22. | -19. | -16. | -13. | -11. | -9. | -8. | -8. | -9. | -11. | -13. |
| 13 | -26. | -29. | -33. | -35. | -38. | -40. | -41. | -42. | -42. | -41. | -39. | -37. | -35. | -32. | -29. | -26. | -23. | -21. | -19. | -18. | -18. | -19. | -21. | -24. |
| 14 | -37. | -40. | -43. | -46. | -48. | -50. | -51. | -52. | -52. | -51. | -50. | -48. | -45. | -42. | -39. | -35. | -33. | -31. | -29. | -28. | -28. | -29. | -31. | -34. |
| 15 | -47. | -50. | -53. | -56. | -58. | -60. | -61. | -62. | -62. | -61. | -60. | -58. | -56. | -53. | -50. | -45. | -43. | -41. | -39. | -38. | -38. | -40. | -41. | -44. |
| 16 | -58. | -61. | -64. | -67. | -69. | -70. | -71. | -72. | -72. | -71. | -70. | -68. | -66. | -63. | -60. | -57. | -54. | -51. | -49. | -48. | -48. | -50. | -52. | -54. |
| 17 | -69. | -72. | -75. | -78. | -80. | -81. | -81. | -82. | -82. | -81. | -80. | -79. | -77. | -75. | -72. | -68. | -65. | -62. | -59. | -58. | -59. | -60. | -62. | -65. |
| 18 | 999. | 999. | 999. | 999. | 999. | 999. | 999. | 999. | 999. | 999. | 999. | 999. | 999. | 999. | 999. | 999. | -75. | -73. | -70. | -68. | -68. | -70. | -74. | -80. |
| 19 | 999. | 999. | 999. | 999. | 999. | 999. | 999. | 999. | 999. | 999. | 999. | 999. | 999. | 999. | 999. | 999. | 999. | 999. | 999. | 999. | 999. | 999. | 999. | 999. |

TABLE I-3

of a few tenths of megahertz at the equator where the north-south gradients of foF2 are the largest. When a large sample of observations was used in the analysis, the final maps produced using the two different coordiante systems were in agreement with each other to better than 5% except at the equator were the differences between grid points were less than 10%.

The second method for making a prediction for the behavior of F2 layer makes use of both the immediate past observations of foF2 and the modeling procedure we use for updating current maps. We assume that data were available at particular locations at the same hour for which we wish to make a prediction for the preceding five days. We use the short term prediction scheme for foF2 described by Rush and Gibbs [2]. The five day weighted mean prediction, Do, is given by

$$D_0 = (5D_{-1} + 4D_{-2} + 3D_{-3} + 2D_{-4} + D_{-5}) \frac{1}{15} \qquad (14)$$

where $D_i$ is the value of foF2 for the $i^{th}$ day preceding the prediction day. All the $D_i$'s are for the same local time at a station location. The set of $D_0$'s represent a prediction at particular locations on the globe. We use our modeling procedure to extend the influence of this set of isolated predictions to other points on the globe. The ITS median ionosphere is updated by the individual predictions to produce a global prediction grid.

The two prediction techniques have been tested using foF2 data available for the years 1960, 1962, 1966 and 1968. The stations used for 1960 are shown on the global map of figure I-3 and listed in table I-4. The results we present here are for an entirely different method of selecting the sets of stations to be used for modeling and verification. With the 1958 data, we choose these sets in a random manner so that each set of stations would give approximate uniform coverage of the globe. For this selection procedure, we observed that the updating analysis produced an foF2 which

Modeling and Verification Stations for 1960

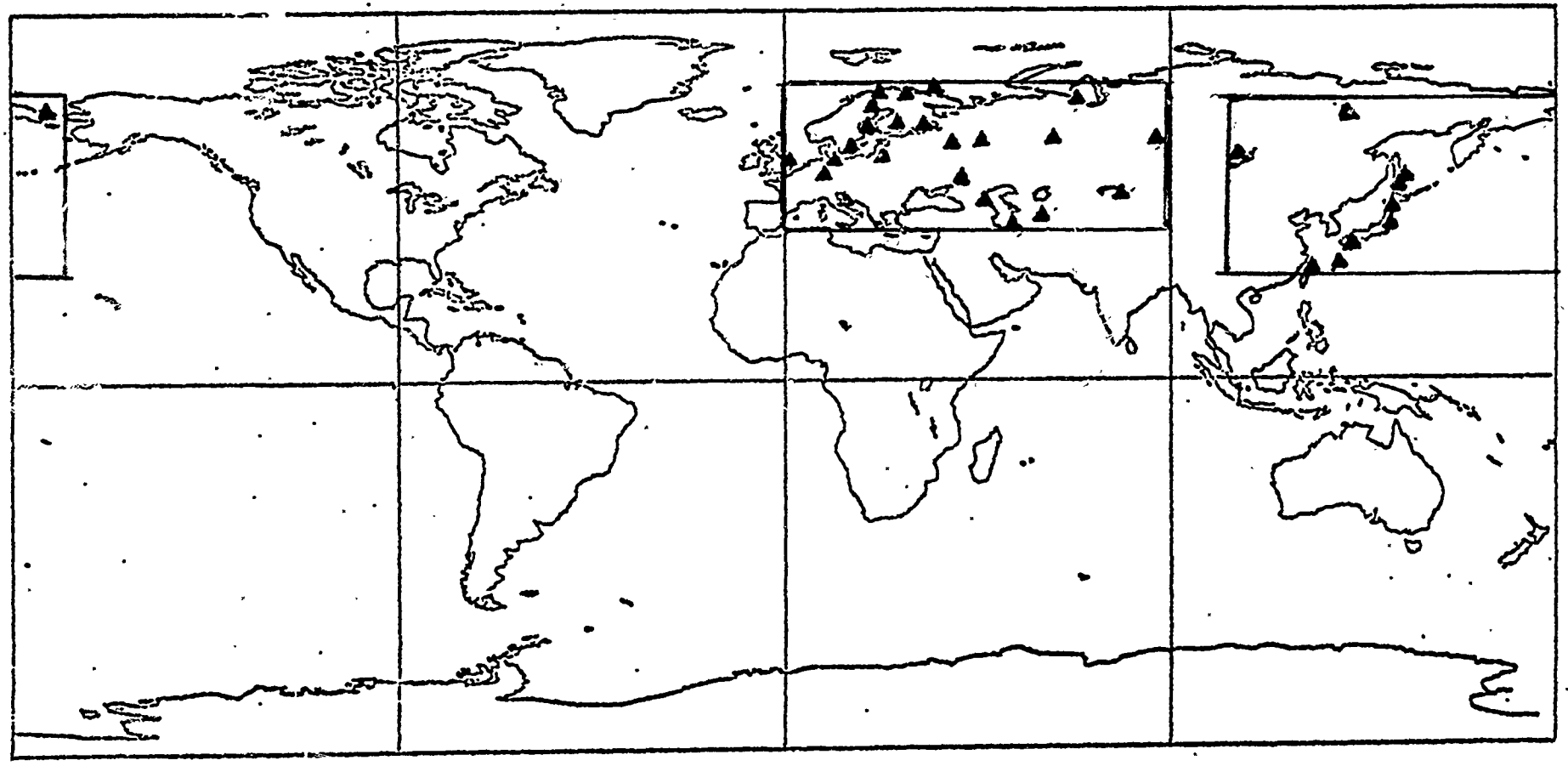

Figure I-3

| Modeling Stations | | | Verification Stations | | |
|---|---|---|---|---|---|
| Station Code | Longitude | Latitude | Station Code | Longitude | Latitude |
| 041 | 12.500 | 41.800 | 352 | 104.000 | 52.500 |
| 048 | 7.600 | 48.100 | 424 | 121.200 | 25.000 |
| 050 | 10.100 | 51.600 | 426 | 127.800 | 26.300 |
| 051 | -.600 | 51.500 | 431 | 130.600 | 31.200 |
| 052 | 14.600 | 50.000 | 462 | 129.700 | 62.000 |
| 055 | 13.400 | 54.600 | 535 | 139.500 | 35.700 |
| 138 | 23.600 | 38.000 | 539 | 140.100 | 39.700 |
| 142 | 44.800 | 41.700 | 545 | 141.700 | 45.400 |
| 145 | 20.500 | 44.800 | 547 | 143.000 | 47.000 |
| 149 | 39.700 | 47.200 | 664 | -173.400 | 64.400 |
| 152 | 21.200 | 52.200 | | | |
| 155 | 37.300 | 55.500 | | | |
| 156 | 44.300 | 56.100 | | | |
| 158 | 17.600 | 59.800 | | | |
| 159 | 24.600 | 60.500 | | | |
| 160 | 30.700 | 60.000 | | | |
| 164 | 18.800 | 64.700 | | | |
| 166 | 26.600 | 67.400 | | | |
| 167 | 20.400 | 67.800 | | | |
| 168 | 33.000 | 69.000 | | | |
| 236 | 51.400 | 35.700 | | | |
| 237 | 58.300 | 37.900 | | | |
| 256 | 61.000 | 56.700 | | | |
| 266 | 66.500 | 66.500 | | | |
| 343 | 76.900 | 43.200 | | | |
| 356 | 84.900 | 56.500 | | | |

TABLE I-4

significantly reduced the residuals at each of the two sets of stations. For the 1960 data, we chose as our modeling stations all those that were west of 90°E longitude and as our verification stations all those that were east of 90°E longitude. This selection should give some indication of how good the modeling procedure is in regions far removed from observations.

The first step when using the five day weighted mean (FDWM) scheme is to produce a map using the median model as a first guess. We have used the data of the 24 hours of January 14, 1960 as a test case. For this test period, approximately 19 stations reported FDWM data for modeling (M) and 10 stations reported FDWM data for verification(V). The results of this analysis are presented in Table I-5. We first note that the values of the RMS residuals for the first guess for all of the hours for both sets of stations is less than that for daily data. Here the average RMS is approximately 1 Mhz whereas for the daily data of 1958 it was greater than 2 Mhz. The FDWM data is in much better agreement with the median model than the daily data. After the updating procedure was applied, the RMS residual for the modeling stations was reduced to less than 0.5 Mhz while the RMS residual for the verification stations shows a smaller reduction for approximately 70% of the hours studied. This improvement is realized inspite of the large north-south gradients (a 10 Mhz change in 40° latitude) observed in the verification data including stations reporting from within the equitorial anomaly region. Table I-6 shows the results for one of the hours for each station. This indicates that it is possible to obtain an improvement in our knowledge of foF2 at a particular time in areas where observations are not readily available. The final grid maps for each of the hours can now be used as a prediction field for the following day.

We use the hourly measurements of foF2 for January 15, 1960 for both modeling and verification stations to study the three methods of making a prediction for foF2. The two grid field methods we have just described can each be used in several ways. The updated FDWM field could be used

RMS Residuals

Five Day Weighted Mean Data

January 14, 1960

| Universal Time | First Guess (Median Model) | | Final Map | |
|---|---|---|---|---|
| | M | V | M | V |
| 000 | 1.0 | 1.4 | 0.3 | 1.7 |
| | 1.1 | 1.2 | 0.5 | 1.1 |
| 200 | 1.1 | 0.7 | 0.5 | 0.8 |
| | 1.0 | 0.9 | 0.5 | 1.1 |
| 400 | 1.0 | 0.8 | 0.6 | 0.9 |
| | 0.9 | 0.7 | 0.5 | 0.7 |
| 600 | 0.9 | 0.8 | 0.4 | 0.7 |
| | 0.8 | 1.0 | 0.5 | 0.9 |
| 800 | 0.8 | 1.0 | 0.4 | 0.8 |
| | 0.7 | 0.9 | 0.4 | 0.9 |
| 1000 | 0.9 | 0.7 | 0.3 | 1.2 |
| | 1.0 | 0.8 | 0.5 | 0.9 |
| 1200 | 1.0 | 0.9 | 0.5 | 0.8 |
| | 1.0 | 0.9 | 0.4 | 0.7 |
| 1400 | 0.9 | 0.8 | 0.5 | 0.6 |
| | 0.9 | 0.9 | 0.3 | 0.8 |
| 1600 | 0.9 | 0.8 | 0.5 | 0.7 |
| | 0.8 | 0.8 | 0.3 | 0.6 |
| 1800 | 0.9 | 0.9 | 0.4 | 0.7 |
| | 0.9 | 0.8 | 0.3 | 0.6 |
| 2000 | 0.9 | 0.9 | 0.6 | 0.9 |
| | 1.0 | 1.0 | 0.2 | 1.2 |
| 2200 | 0.9 | 1.0 | 0.5 | 1.0 |
| | 1.1 | 1.2 | 0.4 | 1.3 |

Table I-5

TABLE I-6

MEASURED DATA JAN 14 13.0 GMT SSN=145. XKP= 3. WO= 190.

MODEL IS ITS COEFFICIENTS

Modeling Stations

| DAY | LT | CODE | NAME | LONG | LAT | Median MODEL | MEAS | Residual | | | Final Map | Meas | Residual |
|---|---|---|---|---|---|---|---|---|---|---|---|---|---|
| 0 14 | 13 | 041 | | 12.500 | 41.800 | 3.439 | 0.000 | 0.000 | 1 | 048 | 12.229 | 12.160 | .069 |
| 1 14 | 13 | 048 | | 7.600 | 48.100 | 11.088 | 12.160 | -1.072 | 2 | 050 | 11.895 | 12.300 | -.405 |
| 2 14 | 13 | 050 | | 10.100 | 51.600 | 10.929 | 12.300 | -1.371 | 3 | 051 | 12.224 | 12.486 | -.262 |
| 3 14 | 13 | 051 | | -.600 | 51.500 | 10.923 | 12.486 | -1.562 | 4 | 052 | 11.833 | 11.728 | .105 |
| 4 14 | 13 | 052 | | 14.600 | 50.000 | 10.967 | 11.728 | -.760 | 5 | 055 | 11.600 | 12.120 | -.520 |
| 5 14 | 13 | 055 | | 13.400 | 54.600 | 10.671 | 12.120 | -1.449 | 6 | 149 | 10.515 | 10.400 | .115 |
| 5 14 | 14 | 138 | | 23.600 | 38.000 | 10.671 | 0.000 | -1.449 | 7 | 152 | 11.383 | 11.200 | .183 |
| 5 14 | 15 | 142 | | 44.800 | 41.700 | 10.671 | 0.000 | -1.449 | 8 | 155 | 10.035 | 10.495 | -.460 |
| 5 14 | 14 | 145 | | 20.500 | 44.800 | 10.671 | 0.000 | -1.449 | 9 | 158 | 11.139 | 11.576 | -.437 |
| 6 14 | 15 | 149 | | 39.700 | 47.200 | 10.135 | 10.400 | -.265 | 10 | 159 | 10.465 | 10.700 | -.235 |
| 7 14 | 14 | 152 | | 21.200 | 52.200 | 10.728 | 11.200 | -.472 | 11 | 150 | 10.226 | 10.438 | -.213 |
| 8 14 | 15 | 155 | | 37.300 | 55.500 | 9.773 | 10.495 | -.722 | 12 | 154 | 9.205 | 8.686 | .520 |
| 8 14 | 15 | 156 | | 44.300 | 56.100 | 9.773 | 0.000 | -.722 | 13 | 156 | 7.780 | 8.550 | -.770 |
| 9 14 | 14 | 158 | | 17.600 | 59.600 | 9.926 | 11.576 | -1.648 | 14 | 157 | 7.917 | 7.353 | .564 |
| 10 14 | 14 | 159 | | 24.600 | 60.500 | 9.650 | 10.700 | -1.050 | 15 | 168 | 6.862 | 6.463 | .400 |
| 11 14 | 15 | 160 | | 30.700 | 60.000 | 9.517 | 10.436 | -.921 | 16 | 256 | 7.630 | 7.795 | -.165 |
| 12 14 | 14 | 164 | | 18.800 | 64.700 | 5.912 | 8.686 | .225 | 17 | 265 | 5.333 | 4.940 | .393 |
| 13 14 | 14 | 166 | | 25.600 | 67.400 | 8.069 | 8.550 | -.481 | 18 | 343 | 7.544 | 7.471 | .073 |
| 14 14 | 14 | 167 | | 20.400 | 67.800 | 8.100 | 7.353 | .747 | 19 | 356 | 5.016 | 4.805 | .211 |
| 15 14 | 15 | 168 | | 33.000 | 69.000 | 7.447 | 6.463 | .985 | | | | | |
| 15 14 | 15 | 236 | | 51.400 | 35.700 | 7.447 | 0.000 | .985 | | | | | |
| 15 14 | 15 | 237 | | 58.300 | 37.900 | 7.447 | 0.000 | .985 | | | | | |
| 16 14 | 17 | 256 | | 61.000 | 56.700 | 7.679 | 7.795 | -.116 | | | | | |
| 17 14 | 17 | 266 | | 66.500 | 66.500 | 6.055 | 4.940 | 1.115 | | | | | |
| 18 14 | 18 | 343 | | 76.900 | 43.200 | 5.520 | 7.471 | -.951 | | | | | |
| 19 14 | 18 | 356 | | 84.900 | 55.500 | 5.189 | 4.805 | .384 | | | | | |

Verification Stations

| | | | | | | | | | | | | | |
|---|---|---|---|---|---|---|---|---|---|---|---|---|---|
| 20 14 | 19 | 352 | | 104.000 | 52.500 | 7.637 | 3.875 | -.238 | 20 | 352 | 3.775 | 3.876 | -.101 |
| 21 14 | 21 | 424 | | 121.200 | 25.000 | 10.955 | 10.205 | .750 | 21 | 424 | 10.716 | 10.205 | .512 |
| 22 14 | 21 | 426 | | 127.800 | 26.300 | 9.433 | 8.405 | 1.028 | 22 | 426 | 9.687 | 8.405 | 1.283 |
| 23 14 | 21 | 431 | | 130.600 | 31.200 | 5.965 | 6.057 | .009 | 23 | 431 | 7.270 | 6.057 | 1.213 |
| 24 14 | 21 | 462 | | 129.700 | 62.000 | 3.255 | 2.614 | .641 | 24 | 462 | 3.178 | 2.614 | .554 |
| 25 14 | 22 | 539 | | 140.100 | 39.700 | 3.194 | 4.205 | -1.011 | 25 | 539 | 4.144 | 4.205 | -.051 |
| 26 14 | 22 | 545 | | 141.700 | 45.400 | 2.847 | 3.729 | -.882 | 26 | 545 | 3.693 | 3.729 | -.035 |
| 27 14 | 22 | 547 | | 143.000 | 47.000 | 2.859 | 3.838 | -.979 | 27 | 547 | 3.605 | 3.838 | -.233 |
| 28 14 | 22 | 535 | | 139.500 | 35.700 | 3.993 | 4.821 | -.828 | 28 | 535 | 5.414 | 4.821 | .593 |
| 29 14 | 2 | 664 | | -173.400 | 64.400 | 3.802 | 3.283 | .518 | 29 | 664 | 4.284 | 3.283 | 1.000 |

as a prediction for more than one day in the future and the maps obtained by modeling in the mixed coordinate system could be rotated n15° for a $n^{th}$ hour in the future prediction. We present here only the closest time internal application of both schemes. In addition, we present the prediction obtained using the median model for comparison. This model requires the smoothed sunspot number to calculate a value of foF2. The two grid field maps are used without any modification based upon any additional knowledge of ionospheric activity.

The RMS residuals for the three methods for the 24-hour period are given in Table I-7. As a prediction, there should be no difference between the modeling and verification stations using the median model. The consistently large residuals from the verification stations must be due to local dynamic effects in the ionosphere. For this reason, we only compare the predictions for each set of stations separately. For almost all of the hours, there is no significant difference between the three predictions for the verification stations. For the modeling stations, there is some slight improvement over the median model by the two grid predictors for a few of the hours. But even here, no systematic behavior is observed. Other modifications to the modeling procedure might improve the prediction capability of the five-day weighted mean data. A more detailed study of the prediction capability of our modeling procedure is given in reference 4. Here, it is shown that one can improve upon the median specification of the F2 region in the midlatitude ionosphere. As we stated earlier, the analysis of the F2 region has been coupled with a vertical electron density model to produce a complete three dimensional ionospheric model which is currently being used in a variety of communication applications.

RMS Residuals for Various Predictions of foF2

| Universal Time | January 15 First Guess FDWM | | January 15 First Guess ITS | | January 15 First Guess Rotated 1 Hour | |
|---|---|---|---|---|---|---|
| | M | V | M | V | M | V |
| 000 | 1.1 | 2.3 | 1.5 | 2.4 | 1.5 | 2.3 |
| | 1.4 | 1.8 | 1.6 | 2.0 | 0.8 | 1.7 |
| 200 | 1.0 | 1.6 | 1.0 | 1.4 | 1.1 | 1.3 |
| | 1.1 | 1.7 | 1.2 | 1.7 | 1.1 | 1.7 |
| 400 | 1.0 | 1.9 | 1.2 | 1.7 | 1.0 | 2.1 |
| | 0.9 | 1.6 | 1.4 | 1.6 | 2.0 | 2.5 |
| 600 | 1.4 | 2.4 | 1.7 | 2.3 | 2.6 | 2.2 |
| | 1.5 | 1.9 | 1.6 | 1.7 | 1.3 | 1.8 |
| 800 | 1.4 | 1.8 | 1.4 | 1.0 | 0.8 | 2.2 |
| | 1.1 | 1.7 | 1.1 | 1.1 | 0.7 | 2.0 |
| 1000 | 1.0 | 1.3 | 1.0 | 1.2 | 1.1 | 1.5 |
| | 0.9 | 1.3 | 1.3 | 1.6 | 1.2 | 1.4 |
| 1200 | 0.7 | 2.6 | 1.1 | 2.6 | 0.8 | 2.4 |
| | 0.6 | 2.2 | 1.1 | 2.3 | 0.9 | 2.1 |
| 1400 | 1.5 | 2.5 | 1.8 | 2.6 | 1.5 | 2.1 |
| | 0.9 | 2.0 | 1.2 | 2.1 | 0.8 | 1.7 |
| 1600 | 0.7 | 2.7 | 0.8 | 2.8 | 0.9 | 2.5 |
| | 0.7 | 1.5 | 0.8 | 1.6 | 0.6 | 1.6 |
| 1800 | 1.1 | 1.1 | 0.7 | 1.2 | 0.5 | 1.1 |
| | 0.7 | 1.1 | 0.6 | 1.1 | 0.7 | 1.1 |
| 2000 | 0.5 | 1.1 | 0.7 | 1.2 | 0.6 | 1.1 |
| | 0.8 | 1.2 | 0.9 | 1.1 | 0.9 | 1.1 |
| 2200 | 1.0 | 1.1 | 0.9 | 1.1 | 0.9 | 1.4 |
| | 1.3 | 1.6 | | | 0.9 | 1.5 |

Table I-7

## REFERENCES


1. Miller, D. C. and Gibbs, J. (1974) Ionospheric Analysis and Ionospheric Modeling, AFCRL-TR-74-0364.

2. Rush, C. M. and Gibbs, J. (1973) Predicting the Day-to-Day Variability of the Mid-latitude Ionosphere for Applications to HF Propagation Prediction, Air Force Surveys in Geophysics, No. 268
AFCRL-TR-73-0335

3. Jones, W. B., and Gallet, R. M., (1962) Representation of divinal and geographic variations of ionospheric data by numerical methods, ITU Tellecomm.
Jour. 29, 129-149

4. Edwards, W. R., Rush, C. M. and Miller, D. C. (1975) Studies on the Development of an Automated Objective Ionospheric Mapping Technique, Air Force Surveys in Geophysics No. 302
AFCRL-TR-75-0124

## II. STUDIES IN POLAR IONOSPHERIC MODELING

In this section we will describe some attempts at improving our knowledge of the F2 region of the polar ionosphere through the use of empirical models. Reference (1) describes some recent work performed toward this end and our approach reflects the same requirements that are described in that report. Our prime requirement is the accuracy of specifying the behavior of foF2 in the polar region as a function of time and other physical parameters. This model can then be used with other ionospheric parameters to predict the three dimensional distribution of electron density and aid in the evaluation of systems employing radio propagation through the ionosphere. The work described here has concentrated on improving our knowledge of foF2 and has made use of several of the presently used empirical models of the ionosphere[1][2].

The most widely used of these models is the ITS monthly median model[2] which represents the median behavior of foF2 (and other ionospheric parameters) in terms of a spherical harmonic expansion in terms of universal time and spatial coordinates. The representation is of the form

$$foF2 = \sum_{k=0}^{N} D_k(T)\, G_k(\phi, \lambda) \quad \text{where } \phi \text{ and}$$

$\lambda$ are the geographic longitude and latitude and T is the universal time. Here the diurnal variation has been separated from the spatial variation and the cutoff parameter of the series, N is equal to 75. The time dependent functions are expanded in a Fourier series containing six harmonics:

$$D_k(T) = A_o^{(k)} + \sum_{j=1}^{G} \left(A_j^{(k)} \cos jT + B_j^{(k)} \sin jT\right).$$

This results in a function

$$foF2 = \sum_{k=0}^{N} A_0^{(k)} G_k(\phi, \lambda) +$$

$$\sum_{k=0}^{N} \sum_{j=1}^{6} (A_j^{(k)} \cos(jT) G_k(\phi,\lambda) + B_j^{(k)} \sin(jT) G_k(\phi, \lambda)]$$

where the $G(\phi, \lambda)$ are linear combinations of surface spherical harmonics. The explicit arguments of the G functions were chosen to be the modified magnetic dip angle which is a function of latitude and the magnetic dip angle I, given by

$$I = \tan^{-1} \left[ \frac{-B_z}{\sqrt{B_x^2 + B_y^2}} \right] \quad \text{where}$$

$B_x$, $B_y$, $B_z$ are the north, east and vertical components of the earth magnetic field vector. The modified magnetic dip angle is then

$$\tan^{-1} \left\{ \frac{I}{\sqrt{\cos \lambda}} \right\}$$

The 988 coefficients were determined using the hourly observations of foF2 that were available from a network of vertical incidence ionosondes for the IGY 1958. The use of additional data from 1964 allowed for the determination of the mean sunspot number dependence of the coefficients.

The methods employed in the development of the monthly median model and the distribution of data tended to give more weight to the low

latitude representation of the ionosphere that than to the high latitude. It has been shown[3] that the true physical variations about the median values of the F2 data in the polar region is much greater than in the midlatitude regions. This has resulted[3] in an improved model for representation of foF2 in the polar region. This model describes the behavior of foF2 in terms of the same coordinates and parameters and does not contain a provision for obtaining a piecewise continuous value of foF2 over the entire globe.

A more recent empirical model of the polar ionosphere is the AFCRL model of Elkins and Rush[1]. This predictive model of the ionosphere is based upon various kinds of data including 1958 and 1964 vertical incidence ionosonde measurements, and optical and satellite observations. The representation of the different regions of the ionosphere range from predominantly statistical models to purely deterministic models. Testing of the entire model has revealed that the greatest need for improvement is in the specification of foF2. We summarize the model for foF2 in the following pages.

The variables and physical parameters used to define foF2 are:

$t$ = local time of day in hours

$t_m$ = corrected magnetic time in hours

$D$ = day of the year (i.e., 1-366)

$\lambda$ = geographic latitude (north)

$\varphi$ = geographic longitude (east)

$\lambda_m$ = corrected geomagnetic latitude (north)

$s$ = sunspot number

$k_p$ = planetary magnetic activity index

$\omega = 2\pi/24$

$u = 2\pi/365$

The value of foF2 is given by

$$f_oF2 = B(D, s) + I(s)\left[c_1 + c_2\left[A_o + 2\sum_{n=1}^{3} A_n \cos(n\omega(t+\phi_n))\right]\right]$$

where

$$B(D, s) = c_3 N(s)\cos(u(D+\rho))$$

$$N(s) = +1 \quad s \geq 100$$

$$N(s) = -1 \quad s < 100.$$

$$I(s) = c_4 + c_5 s + c_6 s^2$$

$$A_o = a_o + a_1\lambda + a_2\lambda\cos(2u(D+t)) + a_3 m(k_p) + a_4 G(\lambda_m, m(k_p), D) + a_5 H(\varphi, D)$$

| | |
|---|---|
| $m(k_p) = 1$ | $k_p < 0.3$ |
| $m(k_p) = 2$ | $0.3 \leq k_p < 1.3$ |
| $m(k_p) = 3$ | $1.3 \leq k_p < 2.3$ |
| $m(k_p) = 4$ | $2.3 \leq k_p < 3.3$ |
| $m(k_p) = 5$ | $3.3 \leq k_p < 4.3$ |
| $m(k_p) = 6$ | $4.3 \leq k_p < 6.3$ |
| $m(k_p) = 7$ | $6.3 \leq k_p$ |

$$G(\lambda_m, m(k_p), D) = p_1 + p_2\lambda_m(3X + \lambda_{m1}(\lambda_{m1} - 1.5S))$$

$$X = \lambda_m^{A_o}(\min)\lambda_m^{A_o}(\max)$$

$$S = \lambda_m^{A_o}(\min) + \lambda_m^{A_o}(\max)$$

$$\lambda_m^{A_o}(\max) = q_4 + q_5\cos(2uD)$$

$$\lambda_m^{A_o}(\min) = q_1 + q_2\, m(k_p) + q_3\cos(\omega(D+\theta_1))$$

$$p_1 = r_1 + r_2\cos(2u(D+\theta_2))$$

$$p_2 = r_3 + r_4\cos(2u(D+\theta_2))$$

$H(\varphi, D) = 0$ $\quad 165^\circ < \varphi \; 195^\circ$ (Pacific Zone)

$H(\varphi, D) = \sum_{n=0}^{4} V_n D^n$ $\quad 195^\circ < \varphi \leq 345^\circ$ (American Zone)

$$H(\varphi, D) = \sum_{n=0}^{4} \omega_n D^n \qquad -15^\circ < \varphi \, 165^\circ \quad \text{(European Zone)}$$

$$A_1 = A_{24} \quad \text{for } \lambda \leq 58^\circ$$

$$A_1 = A_{24}(90. - \lambda)/32. \quad \text{for } \lambda > 58^\circ$$

$$A_{24} = b_o + 2 \sum_{n=1}^{3} b_n \cos(nu(D+\alpha))$$

$$A_2 = d_o + 2 \sum_{n=1}^{3} d_n \cos(nu(D+\delta_n))$$

$$A_3 = e_o + 2 \sum_{n=1}^{3} e_n \cos(nu(D+\epsilon_n))$$

$$\Phi_1 = f_o + 2 \sum_{n=1}^{3} f_n \cos(nu(D+\rho_n))$$

$$\Phi_2 = g_o + 2 \sum_{n=1}^{3} g_n \cos(nu(D+\eta_n))$$

$$\Phi_3 = h_o + 2 \sum_{n=1}^{3} h_n \cos(nu(D+\gamma_n))$$

Auroral Oval Correction to foF2

for $6 \leq t_m < 18$ (magnetic day)

$$f_oF2' = f_oF2(1 - C)\, e^{\frac{-(\lambda_m - \Delta)^2}{6}}$$

where $C = 1 - .35 \cos(\omega(t - \Phi_1))\,(1 + \cos(u(D+8)))/2$

$\Delta = 80 - 1.2k_p$ (magnetic latitude of auroral oval center line for day, Degs.)

for $-6 \leq t_m < 6$

$$f_oF2' = f_oF2 + [k_p/4] \cos(\omega t_m)\, e^{\frac{-(\lambda_m - \beta)^2}{6}}$$

where $\beta = 72 - 1.8k_p + 5.1 \cos(\omega(t_m - 1))$ (magnetic latitude of auroral oval center line for night, Degs.)

## Constants for AFCRL foF2 Polar Model

| | | | |
|---|---|---|---|
| $c_1 = 4.8$ | $a_0 = 0.0$ | $q_1 = 88.5$ | $v_0 = 0.521$ |
| $c_2 = 0.42$ | $a_1 = -0.439 \times 10^{-1}$ | $q_2 = -2.5$ | $v_1 = -0.347 \times 10^{-1}$ |
| $c_3 = 0.6$ | $a_2 = 0.386 \times 10^{-2}$ | $q_3 = 5.0$ | $v_2 = 0.316 \times 10^{-3}$ |
| $c_4 = 1.0$ | $a_3 = -0.424$ | $q_4 = 55.0$ | $v_3 = -0.133 \times 10^{-5}$ |
| $c_5 = 0.12$ | $a_4 = 0.739$ | $q_5 = 2.0$ | $v_4 = 0.142 \times 10^{-8}$ |
| $c_6 = -2.6 \times 10$ | $a_5 = 0.440$ | $r_1 = 3.2$ | $w_0 = 0.963 \times 10^{-1}$ |
| $\rho = 10.0$ | $\Psi = -105.0$ | $r_2 = -4.4$ | $w_1 = -0.101 \times 10^{-1}$ |
| | $\theta_1 = -182.5$ | $r_3 = -1.0 \times 10^{-5}$ | $w_2 = 0.198 \times 10^{-3}$ |
| | $\theta_2 = -90.0$ | $r_4 = 1.5 \times 10^{-5}$ | $w_3 = -0.853 \times 10^{-6}$ |
| | | | $w_4 = 0.106 \times 10^{-8}$ |
| | $b_0 = 1.368$ | | $d_0 = 0.2784$ |
| | $b_1 = 0.589$ | $\alpha_1 = -1.139$ | $d_1 = 0.1263$ |
| $\beta_1 = -15.25$ | $b_2 = 0.449 \times 10^{-1}$ | $\alpha_2 = 113.0$ | $d_2 = 0.6422 \times 10^{-1}$ |
| $\beta_2 = -5.563$ | $b_3 = 0.468 \times 10^{-1}$ | $\alpha_3 = 41.08$ | $d_3 = 0.3222 \times 10^{-1}$ |
| $\beta_3 = -1.458$ | $f_0 = 15.57$ | | $e_0 = 0.1149$ |
| $\epsilon_1 = -19.86$ | $f_1 = 0.6066$ | $\rho_1 = 176.5$ | $e_1 = 0.4306 \times 10^{-1}$ |
| $\epsilon_2 = 97.99$ | $f_2 = 0.2784$ | $\rho_2 = 17.32$ | $e_2 = 0.1186 \times 10^{-1}$ |
| $\epsilon_3 = 51.45$ | $f_3 = 0.2574$ | $\rho_3 = 68.02$ | $e_3 = 0.1739 \times 10^{-1}$ |
| | $g_0 = -0.1236$ | $\eta_1 = 1.379$ | $h_0 = 1.511$ |
| $\gamma_1 = 2.221$ | $g_1 = 1.112$ | $\eta_2 = 7.242$ | $h_1 = 1.325$ |
| $\gamma_2 = 102.4$ | $g_2 = 0.2338$ | $\eta_3 = 59.09$ | $h_2 = 0.3508$ |
| $\gamma_3 = 2.900$ | $g_3 = 0.2562$ | | $h_3 = 0.2319$ |

TABLE II-1

Both the ITS model and the AFCRL polar model are based largely on the vertical incidence ionosonde data of IGY 1958. The AFCRL model differs from the ITS model in that the daily-hourly observations of foF2 were used rather than the monthly median data for the set of available ionosonde locations. The scale of significant polar ionospheric phenomena both spatially and temporally is smaller than that of the available data and the variability of foF2 as a function of the relevant parameters is so great that the data may be insufficient to specify a model with the correct empirical behavior. The use of the daily data allowed for a description of the planetary magnetic activity index, $K_p$ dependence of foF2 in the AFCRL model. This dependence was coupled to the behavior of the important ionospheric boundaries in the polar region. The improved ITS model is still based upon median data and, therefore, does not contain any $K_p$ dependence. While the first ITS model specifies foF2 on a global scale, the AFCRL model does not contain a provision for predicting foF2 below $45^{\circ}$ north geographic latitude. This tends to be a severe limitation of the model since many applications require knowledge of the ionospheric parameters over a radio wave path spanning different global regions.

Empirical Basis for foF2 Model

In order to determine the behavior of foF2, several sets of ionosonde data were used. Approximately 300,000 hourly values of foF2 for the fifty stations north of $45^{\circ}$ latitude for IGY 1958 constituted the primary data base. In addition, we used the hourly ionsonde data for each day of March, June, September and December of 1964. For some of the study, we used the hourly data for the stations listed in table II-2 for the years 1960, 1962, 1966 and 1968.

The polar ionosphere may be described in terms of several boundaries which display certain regular characteristics. The most notable ones being the trough and the auroral oval. In an attempt to isolate these features from

TABLE II-2

Stations for Which foF2 Data is Available for 1960, 1962, 1966, 1968

| Stations | | $\lambda$ (Degrees) | $\lambda_m$ (Degrees) | $\phi$ (Degrees) |
|---|---|---|---|---|
| Gorky | 156 | 56.2 | 51.6 | 44.3 |
| Julensruk | 055 | 54.6 | 62.5 | 13.4 |
| Kiruna | 167 | 67.8 | 64.3 | 20.5 |
| Leningrad | 160 | 60.0 | 55.8 | 30.3 |
| Lindau | 050 | 51.4 | 48.3 | 10.1 |
| Lycksele | 164 | 64.6 | 61.2 | 18.8 |
| Miedzeszyn | 152 | 52.2 | 48.2 | 21.2 |
| Moscow | 155 | 55.5 | 51.0 | 37.3 |
| Murmansk | 168 | 68.9 | 64.6 | 33.0 |
| Nurmijarvi | 159 | 60.5 | 56.6 | 24.6 |
| Providenya | 664 | 64.4 | 60.3 | 18.5 |
| Sakekhard | 266 | 66.6 | 61.8 | 66.6 |
| Slough | 051 | 51.5 | 49.9 | 359.4 |
| Sodankyla | 166 | 67.4 | 63.4 | 26.6 |
| Uppsala | 158 | 59.8 | 56.4 | 17.6 |
| Yakutsk | 462 | 62.0 | 56.4 | 129.8 |

the other dynamic processes occurring in the ionosphere, we have found it useful to examine the data for various geographic regions separately. We have defined our boundaries by the three parameters: $\theta_A$, the southern boundary (in corrected geomagnetic latitude) of the auroral oval, or equivalently the northern wall of the trough, $\theta_B$, the northern boundary of the auroral oval and $\theta_S$, the southern boundary of the trough. These parameters are given by the following:

Magnetic Day $6.0 < t_{CGM} \leq 18.0$ (where $t_{CGM}$ is the corrected geomagnetic time)

$$\theta_A = 78.0^\circ - 2.5\ K_p \quad \text{(Degrees)}$$

$$\theta_B = 82.0 - 1.5\ K_p$$

$$\theta_S = \theta_A - 6.0^\circ$$

Magnetic Night $t_{CGM} \leq 6.0$ or $t_{CGM} > 18.0$

$$\theta_A = 71.0^\circ - 2.5\ K_p \cos\left\{\frac{\pi}{12}(t_{CGM}-1)\right\})$$

$$\theta_B = 75.0^\circ + (1.0 - 2.5 \cos\left\{\frac{\pi}{12}(t_{CGM}-1)\right\} K_p$$

$$\theta_S = \theta_A - 6.0^\circ$$

Using these boundaries, we refer to the data as belonging to one of the following regions:

a) $\lambda_m < \theta_S$ South of the trough (ST)

b) $\theta_S \leq \lambda_m \angle \theta_A$ in the trough (T)

c) $\theta_A \leq \lambda \leq \theta_B$ in the auroral oval (A)

d) $\theta_B < \lambda_m$ north of the auroral oval (NA)

where $\lambda_m$ is the corrected geomagnetic latitude of the station. We also treat the data as occurring during the solar day when $\chi$ (solar zenith angle) $\leq 94.6^\circ$ and solar night $\chi > 94.6^\circ$. An indication of the distribution of foF2 observations can be seen from the 1958 data. For the daytime auroral region the fraction of total observations for each month varies between a low of 2% during the winter months and a peak of 11% during the summer months. For the nighttime during the summer months, 1% and during the winter months 7% of the data is from the auroral oval region. For the trough, this fraction of monthly data varies between a low of 2% during the summer months to 14% during the winter months. These small figures for 1958 still represent a reasonable amount of data for the study of the behavior of foF2 in the two regions of interest. The problem of having enough useful data is enhanced during the other years under study. The distribution of data for 1960 is shown in the following table.

TABLE II-3

Spatial Distribution of Hourly foF2 Observations for 1960

Number of daily-hourly observations.

| | Solar Day | | | | Solar Night | | | |
|---|---|---|---|---|---|---|---|---|
| | (ST) | (T) | (A) | (NA) | (ST) | (T) | (A) | (NA) |
| January | 2900 | 250 | 0 | 0 | 4300 | 700 | 50 | 0 |
| February | 3600 | 300 | 0 | 0 | 3500 | 600 | 50 | 0 |
| March | 5000 | 400 | 30 | 0 | 2900 | 650 | 50 | 0 |
| April | 5000 | 800 | 100 | 0 | 1800 | 550 | 150 | 0 |
| May | 6700 | 1200 | 150 | 0 | 1300 | 250 | 40 | 0 |
| June | 6800 | 1400 | 100 | 0 | 1000 | 75 | 0 | 0 |
| July | 6800 | 1200 | 125 | 0 | 1200 | 100 | 10 | 0 |
| August | 6000 | 900 | 75 | 0 | 1700 | 325 | 50 | 0 |
| September | 5400 | 480 | 40 | 0 | 2700 | 500 | 60 | 0 |
| October | 4000 | 400 | 100 | 0 | 3100 | 550 | 100 | 0 |
| November | 3100 | 200 | 30 | 0 | 3600 | 600 | 60 | 0 |
| December | 2600 | 200 | 15 | 0 | 4100 | 750 | 90 | 0 |

It should be noted that the placement of each observation depends upon the definition of the boundaries for that hour and hence upon the $K_p$ value. We use for our $K_p$ data base the three hour planetary index. We did not attempt to establish our boundary definitions from the data. Instead, we have concentrated our efforts in trying to extract the behavior of the amplitude of foF2 in the various regions.

Corrections to AFCRL Polar Model

The AFCRL Polar Model for foF2 was an attempt to parameterize the behavior of foF2 in a limited geographic region in terms of the spatial and temporal variables which appear to be related to the dynamic processes occurring in the polar region. As can be seen from the model description,

they can be divided into the following categories:

(1) Geographic latitude and local time

(2) Geomagnetic latitude and geomagnetic time

While the diurnal variation of the model did not predict the sunrise gradients with great accuracy, the largest deviations between the model and the 1958 data were due to the terms depending upon the magnetic coordinates. It was decided to redetermine that part of the model for foF2 which represents the magnetic effects. We used as a starting model, $foF2^m$, that part of the polar model which remains when the term

$$G(\lambda_m, m(k_p), D) = 0$$

and when the two corrections for magnetic day and night are omitted. An examination of the residuals

$$\Delta foF2(t) = foF2^m(t) - OBS(t)$$

at the various ionosonde locations showed the presence of a strong auroral oval during the winter months. The trough was not as clearly defined. The residuals were then assumed to be of the form:

$$\Delta foF2 = (c_0 + c_1 B) + (c_2 + c_3 B + m(c_4 + c_5 B))\lambda_m$$

$$+ (c_6 + c_7 B + m(c_8 + c_9 B))\lambda_m^2$$

$$+ (c_{10} + c_{11} B)\lambda_m^3$$

$$+ (t-to)\{(c_{12} + c_{13} B) + (c_{14} + c_{15} B)\lambda_m + (c_{16} + c_{17} B)\lambda_m^2$$

$$+ (c_{18} + c_{19} B) \lambda_m^3 \}$$

$$+ (t-t_0)^2 \{ (c_{20} + c_{21} B) + (c_{22} + c_{23} B + m (c_{24} + c_{25} B)) \lambda_m$$

$$+ (c_{26} + c_{27} B + m (c_{28} + c_{29} B)) \lambda_m^2$$

$$+ (c_{30} + c_{31}) \lambda_m^3 \}$$

where $B = \cos \left[ \frac{2\pi (D + 8)}{365} \right]$ and $m = m (k_p)$

A multiple linear regression procedure was used with all the daily hourly observations of foF2 for the polar stations for 1958. The results of the analysis were not found to be satisfactory. An examination of the relative regression coefficients $c_4/c_2$, $c_5/c_3$, $c_8/c_6$, $c_9/c_7$, etc. indicated that no dependence upon $k_p$ could be established from this procedure. The $k_p$ indices represent three hour global averages and while they may appear to be correlated with the variation of foF2 at a particular station show little correlation with foF2 at sets of ionosonde locations. The deficiency of the regression technique is attributed to the nonuniformity and sparseness of the data in the geographical region of interest. The residual, $\Delta$foF2 is expected to describe the variation of foF2 in the region of the trough and the auroral oval but as we have already shown less than 10% of the data are from these regions. The regression procedure could only be of value if variable weighting factors could be assigned to each of the observations.

Corrections to the ITS Median Model

The methods employed in the development of the ITS median model for

foF2 tended to give more weight to low and midlatitude observations than to those at high latitude. It has been shown that the resulting numerical maps do not represent the true physical variations of the original data in the polar region[3]. Attempts have been made to improve the representation of ionospheric characteristics in the polar region using different mapping coordinates, but with basically the same mapping functions. An improvement in the representation of foF2 in the polar region was obtained but the resulting model is applicable only above $30^{\circ}$ north latitude.

Since the original global model represents the physical behavior of the ionosphere quite well away from the polar region, we have chosen to use this model as a first approximation to the ionosphere at high latitudes. We have then sought to find corrections to this model to describe the behavior of the high latitude ionosphere in terms of the relevant spatial and geophysical variables. In an attempt to isolate the variation of foF2 with magnetic activity on a global scale, we first studied the data available during the solar day (solar zenith angle, $\chi \leq 94.6^{\circ}$). For each hourly observation of foF2, we have calculated the percent residual:

$$\Delta(t, \phi, \lambda, s, k_p) \equiv \frac{foF2^{ITS}(t, \phi, \lambda, s) - foF2^{obs}}{foF2^{ITS}(t, \phi, \lambda, s)}$$

were s is the mean sunspot number for a given month. In figure II-1, we show $\Delta$ as a function of $m(k_p)$ (as described in the CRL polar model) for each of the months for the 1958 data. The four areas, ST, T, A, and NA, of the polar region are shown as separate curves. The eight months from March through October show a similar linear dependence upon $m(k_p)$ which is independent of $\lambda_m$ for each month. The winter months also exhibit the same behavior except for the region of the auroral oval in which the re-

RESIDUALS FOR 1958 foF2: SOLAR DAY

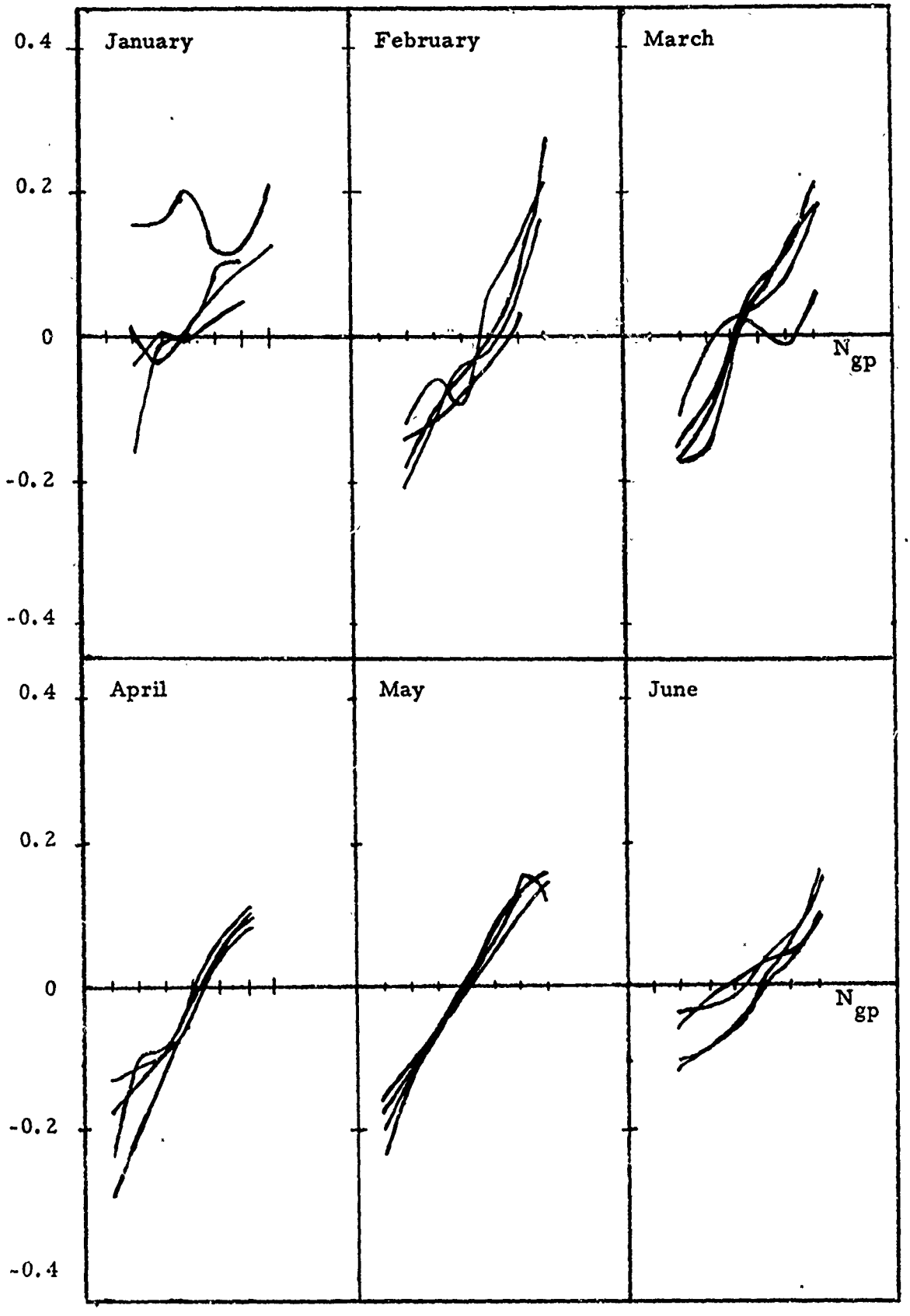


Figure II-1a

RESIDUALS FOR 1958: SOLAR DAY

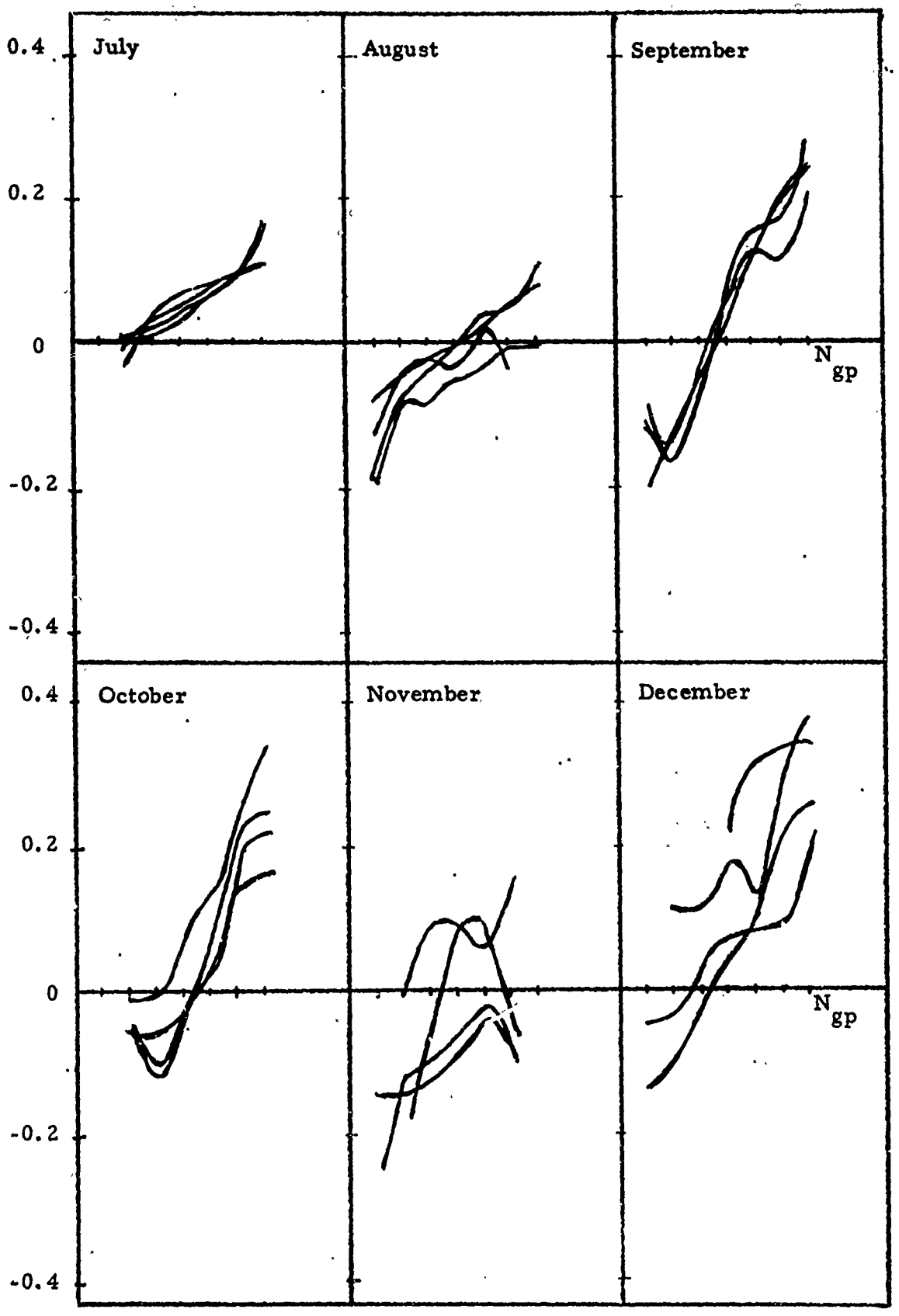


Figure II-1b

quired correction is much larger than for the other regions. It is also important to note that there is very little data available during the solar day for the winter months so that some of these effects may not be statistically significant. The data in each of these months has been separately fit to the function:

$$\Delta_i = a_i + b_i m(k_p) \qquad \text{where i denotes the month.}$$

In figure II-2, we plot $a_i$ and $b_i$ as a function of the month. Both a and b appear to have a six-month period. Superimposed upon the experimental curves are the two expressions:

$$a(D) = -0.155 + 0.095 \cos\left(\frac{4\pi D}{365}\right)$$

$$b(D) = 0.0425 - 0.0225 \cos\left(\frac{4\pi D}{365}\right)$$

where D has been taken to be the middle day of each month. For the low solar activity year, 1964 only four months of data were available. Figure II-3 shows the variation of the residual, $\Delta$, with $m(k_p)$ for the solar day for these four months. Here, we also note only a very small difference between the separate areas within the polar region. If we assume that the period and phase of the a and b parameters are the same for the both years, we can determine the amplitudes for 1964. The correction parameters are:

$$a(D) = -0.133 + 0.078 \cos\left(\frac{4\pi D}{365}\right)$$

and

$$b(D) = 0.0225 - 0.0110 \cos\left(\frac{4\pi D}{365}\right)$$

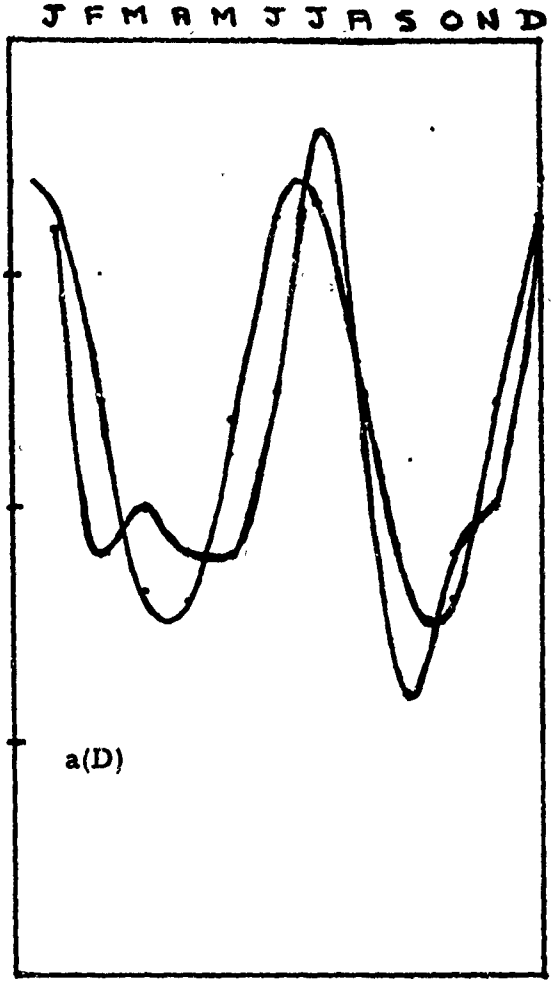


$$\Delta = a(D) + b(D)\, N_{gp}$$

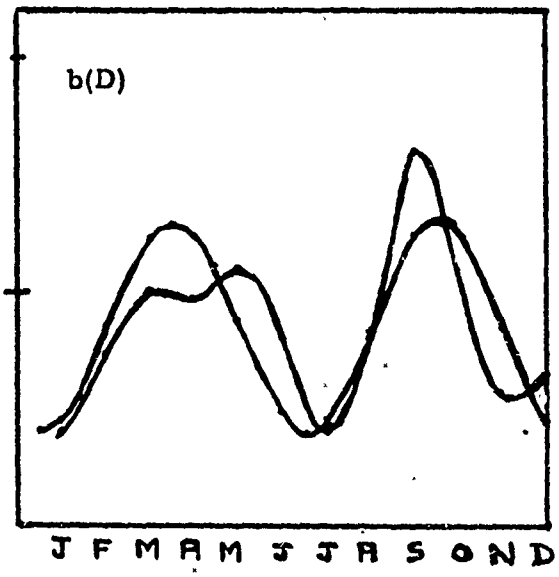


Figure II-2

RESIDUALS FOR 1964 foF2: SOLAR DAY

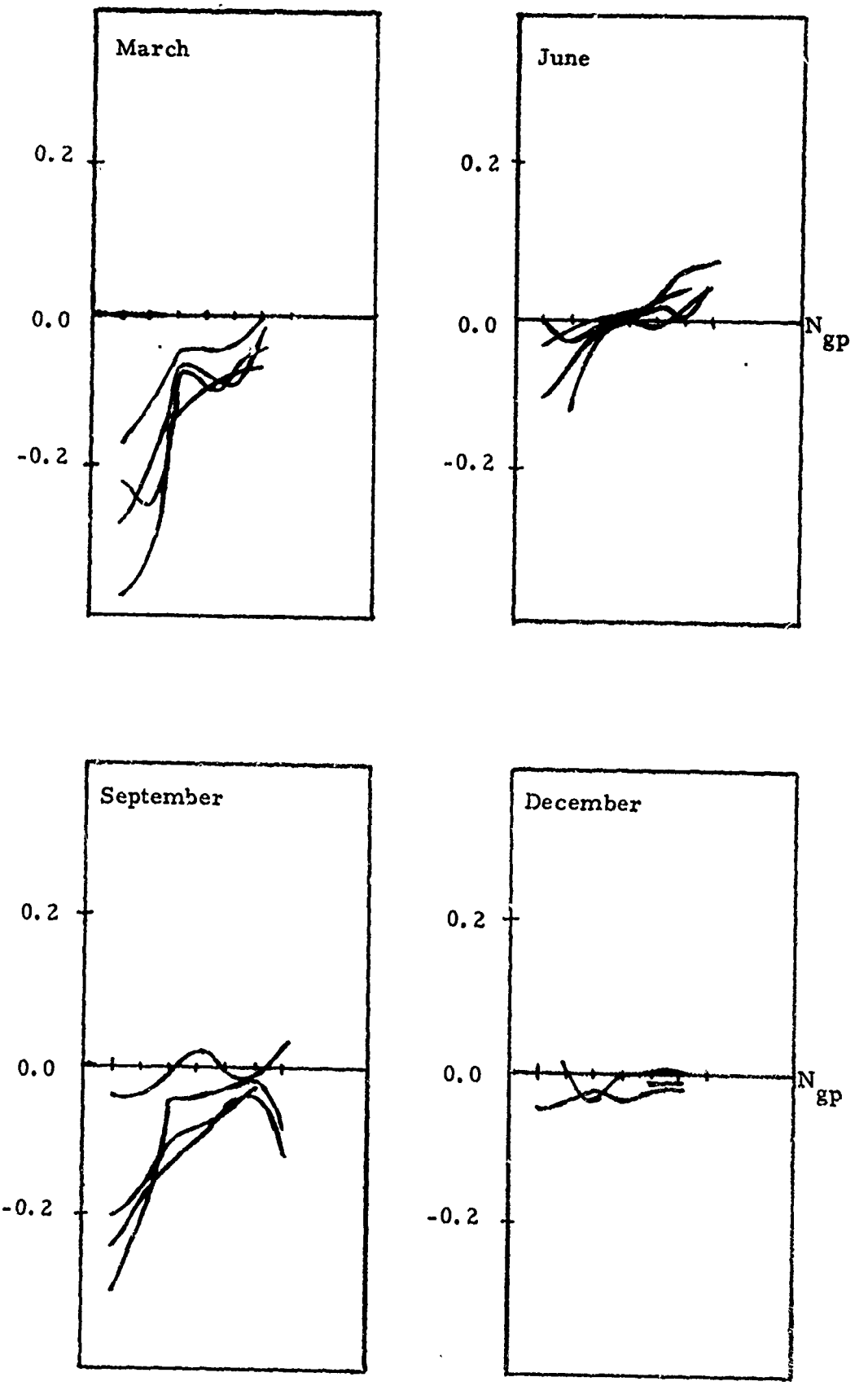


Figure II-3

There is fairly good agreement between the two years for each of the four parameters. The data from each of the other years displays a similar behavior with the value of a being much more irregular than the behavior of b. We consider this to represent a global correction to the ITS model for both day and night which should be applied independent of the polar region. This given as:

$$foF2(\chi \leq 94.6^{o}) = foF2^{ITS} \left\{ 1 - a(D) - b(D)\, m(k_p) \right\} .$$

We have examined the residuals for the solar night for each of the years as a function of month, corrected magnetic latitude, corrected magnetic time and magnetic activity. While the residuals are clearly a function of the corrected magnetic latitude it is difficult to extract any regular variation with the other parameters. In general, we have established the residual in the area south of the trough as a standard for any given month and magnetic activity and sought to obtain corrections in the other regions that are consistent with the dominant morophological features of the ionosphere. Our modeling of both the trough and auroral oval regions are strongly correlated with our assumptions about the location and extent of each of these regions and their dependence upon magnetic activity. It has been observed previously[1] that the data from ground based ionosondes during 1958 do not show strong evidence of the trough. We find this to be true even when the dependence of the nighttime residuals on magnetic activity is also examined.

When the features do occur, we expect to observe the residuals in the trough region to be larger than those of the region used as a standard. Correspondingly, we expect to observe residuals which are lower (ITS model to small) in the auroral oval region than those in standard region. We illustrate periods in which these effects are present with strong intensity

in the following graphs of the residual as a function of magnetic activity ($m(k_p)$).

(1) March and June 1964 figure II-4. ($\chi > 94.6^o$)

(2) March and August 1962 figure II-5.

In each of these months, both features are observed. We have found evidence for a nighttime auroral oval correction in most of the months with it being more intense during the winter. The evidence for the trough is much more sporadic although it appears to be quite weak during the winter. The data does not indicate a strong correlation of the intensity of the two effects with the three-hour planetary index, $k_p$.

From the general features of the residuals, we have assumed corrections to the ITS model during the solar night to be of the form:

$$foF2 = foF2(\chi \leq 94.6^o)\left[1 + \Delta_N\right] \quad \text{where}$$

$$\Delta_N = A_0 \sqrt{\exp}\, x_1 \exp\left\{-x_1^2/2\right\} \text{ for } \lambda_m \geq \phi_A$$

$$\phi_A = 70.2^o - 1.65\, k_p - 5.1 \cos\left[\frac{\pi}{12}(t_{CGM} - 1)\right] \quad \text{(degrees)}$$

$$x_A = 3.7^o + 1.3\, k_p \quad \text{(degrees)}$$

$$x_1 = \frac{(\lambda_m - \phi_A)}{x_A}$$

$$\Delta_N = T\left[1 + \cos\left(\frac{2\pi(D+11)}{365}\right)\right] \quad \text{for} \quad \lambda_m < \phi_A$$

RESIDUALS FOR 1964 foF2: SOLAR NIGHT

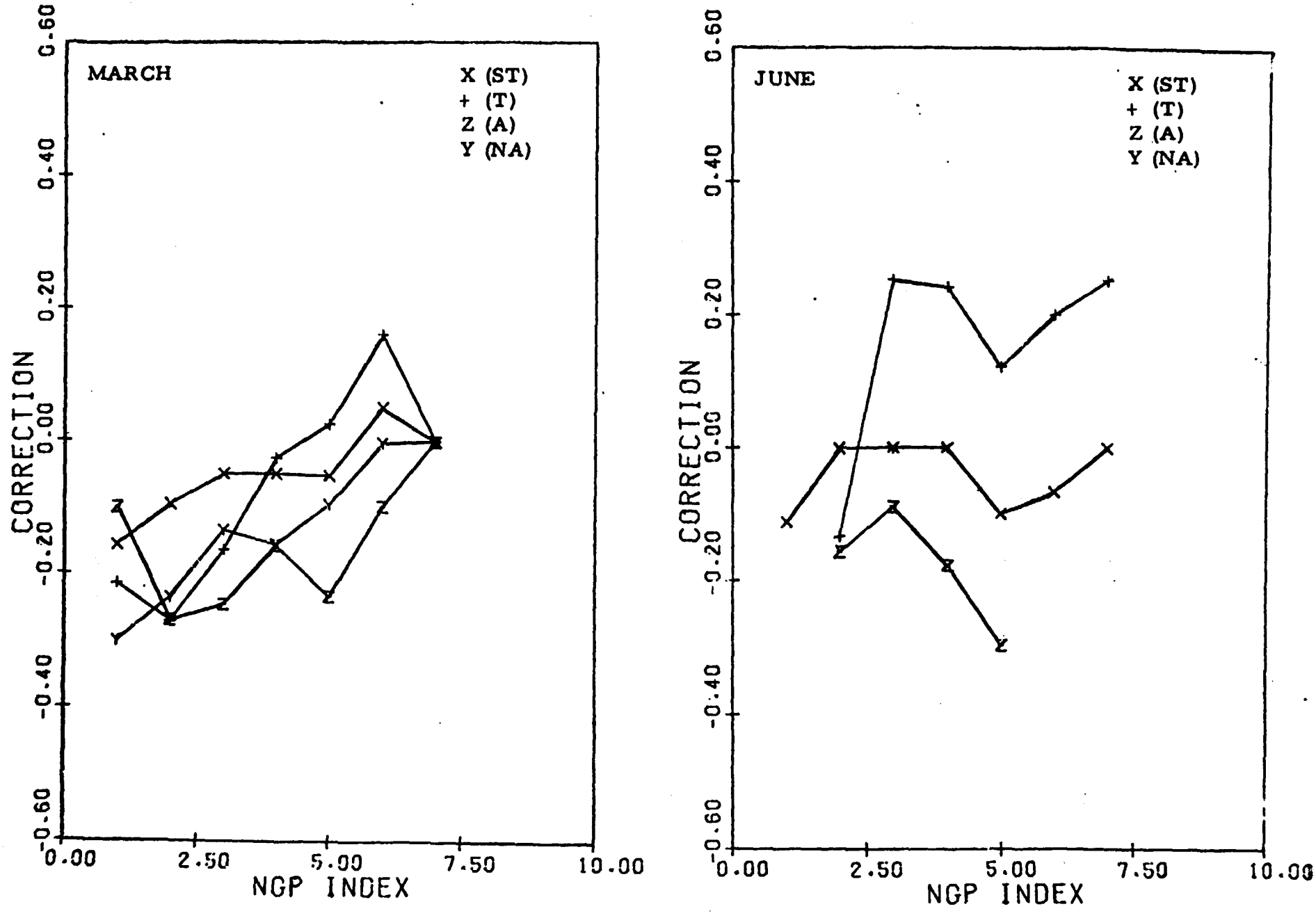


Figure II-4

RESIDUALS FOR 1962 foF2: SOLAR NIGHT

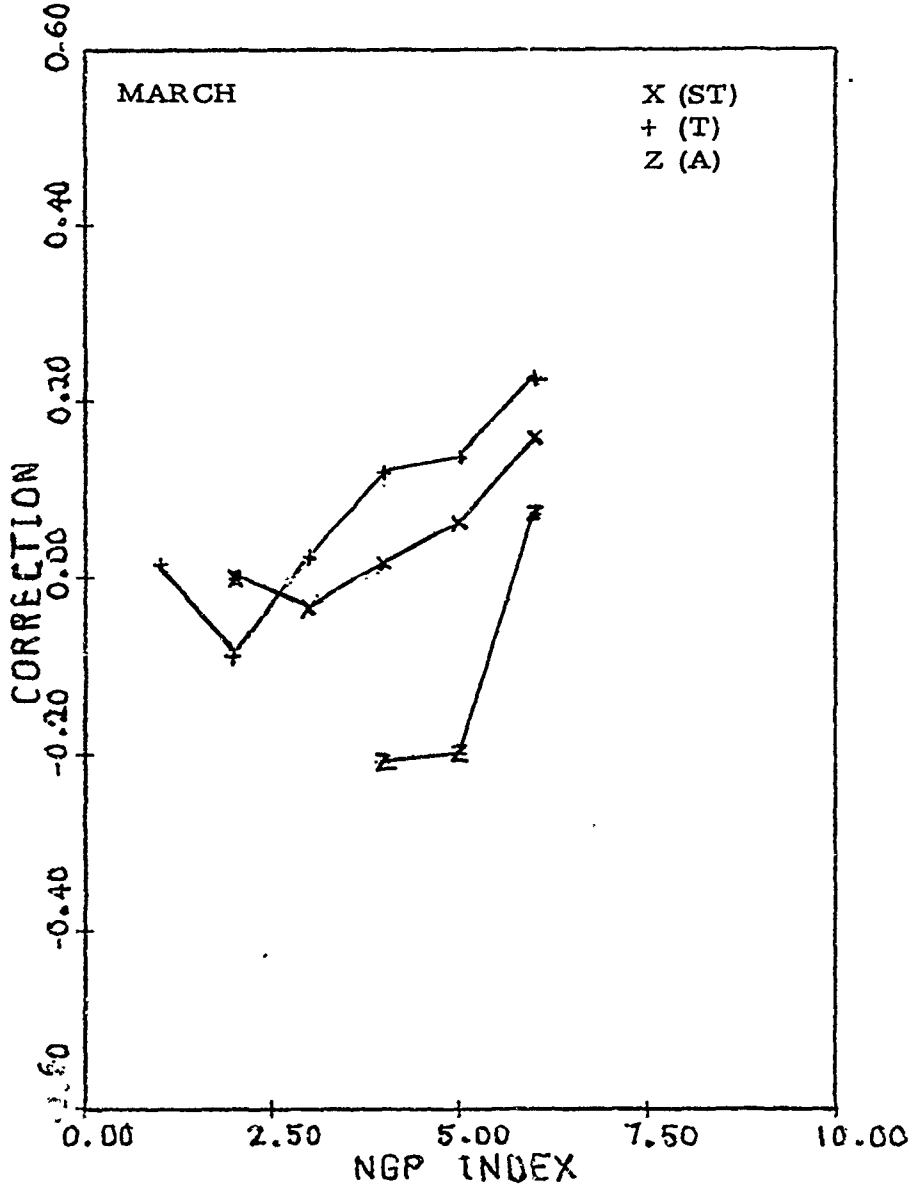


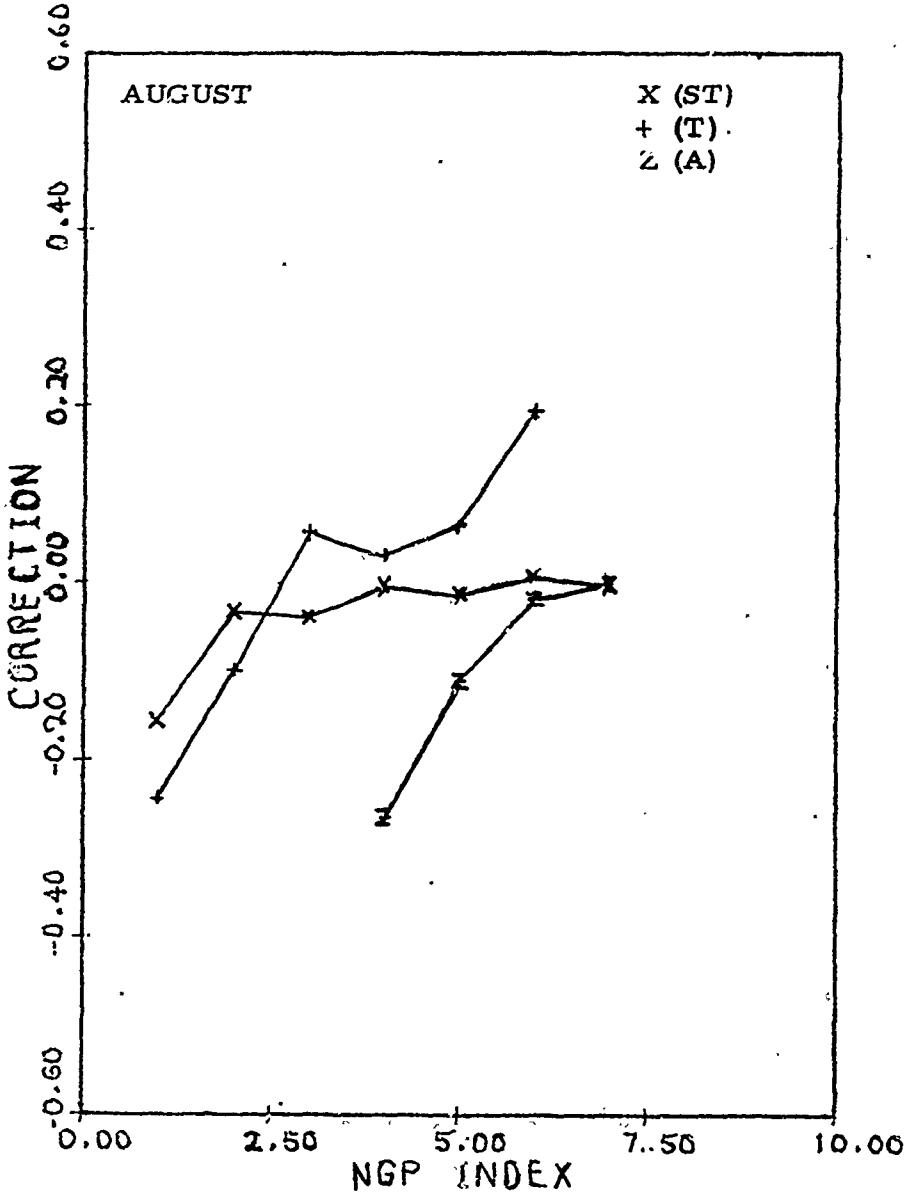


Figure II-5

$$T = T_1 \sqrt{\exp}\ x_1 \exp\left\{-x_1^2/2\right\} \exp\left\{-(t_{CGM} - 3)^2/12\right\}$$

$T_1 = 0$ for $\chi \leq 90^\circ$

or $6.0 < t_{CGM} < 18.0$

$T_1 = T_0$ $\chi > 94.6^\circ$ and $6.0 < t_{CGM} < 18.0$

$$T_1 = T_0 \left\{\frac{\chi - 90^\circ}{4.6^\circ}\right\} \quad 90^\circ \leq \chi \leq 94.6^\circ \text{ and } 6.0 < t_{CGM} < 18.0$$

and where $t_{CGM}$ is the corrected geomagnetic time and $\lambda_m$ is the corrected geomagnetic latitude. The maximum amplitudes have initially been taken to be: $T_0 = -0.20$ and $A_0 = 0.20$. An indication of the magnitude of the correction in the trough region is given in table II-4 where the maximum nighttime values are given for $\lambda_m = \phi_A$ and $t_{CGM} = 3.0$.

TABLE II-4

Ratio of foF2 / foF2 (ITS)

| | Day Ngp | | | Night Ngp | | |
|---|---|---|---|---|---|---|
| Day of Year | 2 | 4 | 6 | 2 | 4 | 6 |
| 0 | 1.02 | 0.98 | 0.94 | 0.612 | 0.588 | 0.564 |
| 91 | 1.12 | 0.99 | 0.86 | 0.896 | 0.792 | 0.688 |
| 182 | 1.02 | 0.98 | 0.94 | 1.02 | 0.98 | 0.94 |
| 273 | 1.12 | 0.99 | 0.86 | 0.896 | 0.792 | 0.688 |
| 365 | 1.02 | 0.98 | 0.94 | 0.612 | 0.588 | 0.564 |

For other values of $\lambda_m$ and $t_{CGM}$ the ratio is between the night and day values. The diurnal variation of foF2 is shown in figure II-6. The curves represent the prediction of the ITS model without corrections and with corrections for $m(k_p)$ values of 2, 4, and 6 for two stations during January 1958. In addition to the spatial independent $k_p$ corrections applied to both locations, the trough correction is clearly apparent in the prediction for Ottawa.

Figures II-7 and II-8 are contour plots of the predictions of foF2 for the two polar models for the region north of $40^o$ N latitude for January 15, 1958 UT = 000 hours. The division between solar day and solar night is explicitly shown ($\chi = 94.6^o$). The second figure contains the corrections to the ITS model that are described above for a $k_p$ value of 1.0. The ITS model is a function of universal time and geographic longitude whereas our polar region corrections are also functions of local time. The entire region shows a general increase in foF2 due to the $k_p$ correction. It should be noted that the model is continuous in foF2 and its first derivations everywhere on the globe. We are now in the process of comparing the model with additional foF2 data with an aim toward a better determination of some of the correction terms.

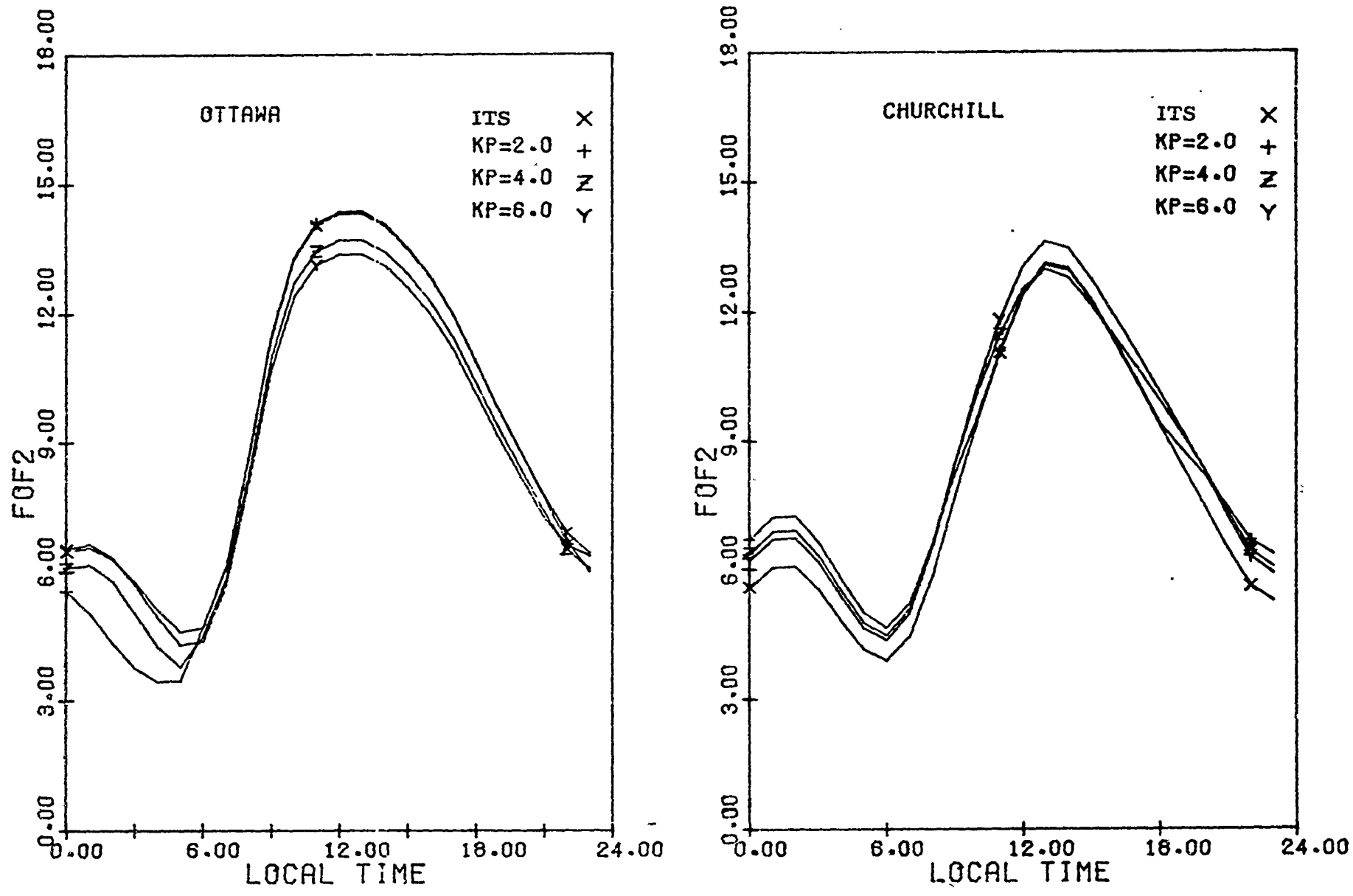


DIURNAL VARIATION OF foF2: ITS MODEL WITH POLAR CORRECTIONS

CONTOUR PLOT OF foF2: POLAR PROJECTION: ITS MODEL

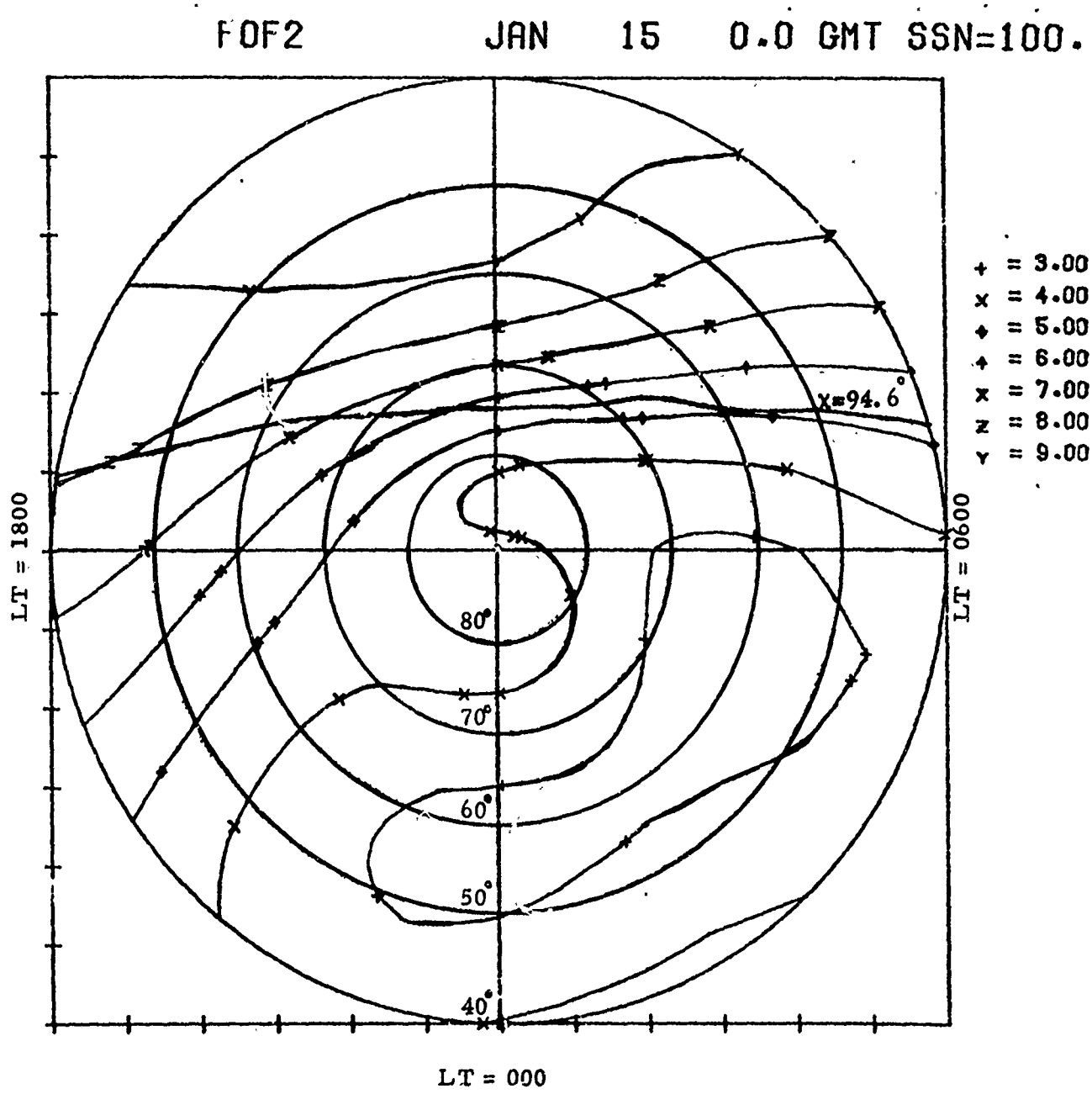


GEOGRAPHIC COORDINATES

Figure II-7

CONTOUR PLOT OF foF2 POLAR PROJECTION

ITS MODEL WITH POLAR CORRECTIONS

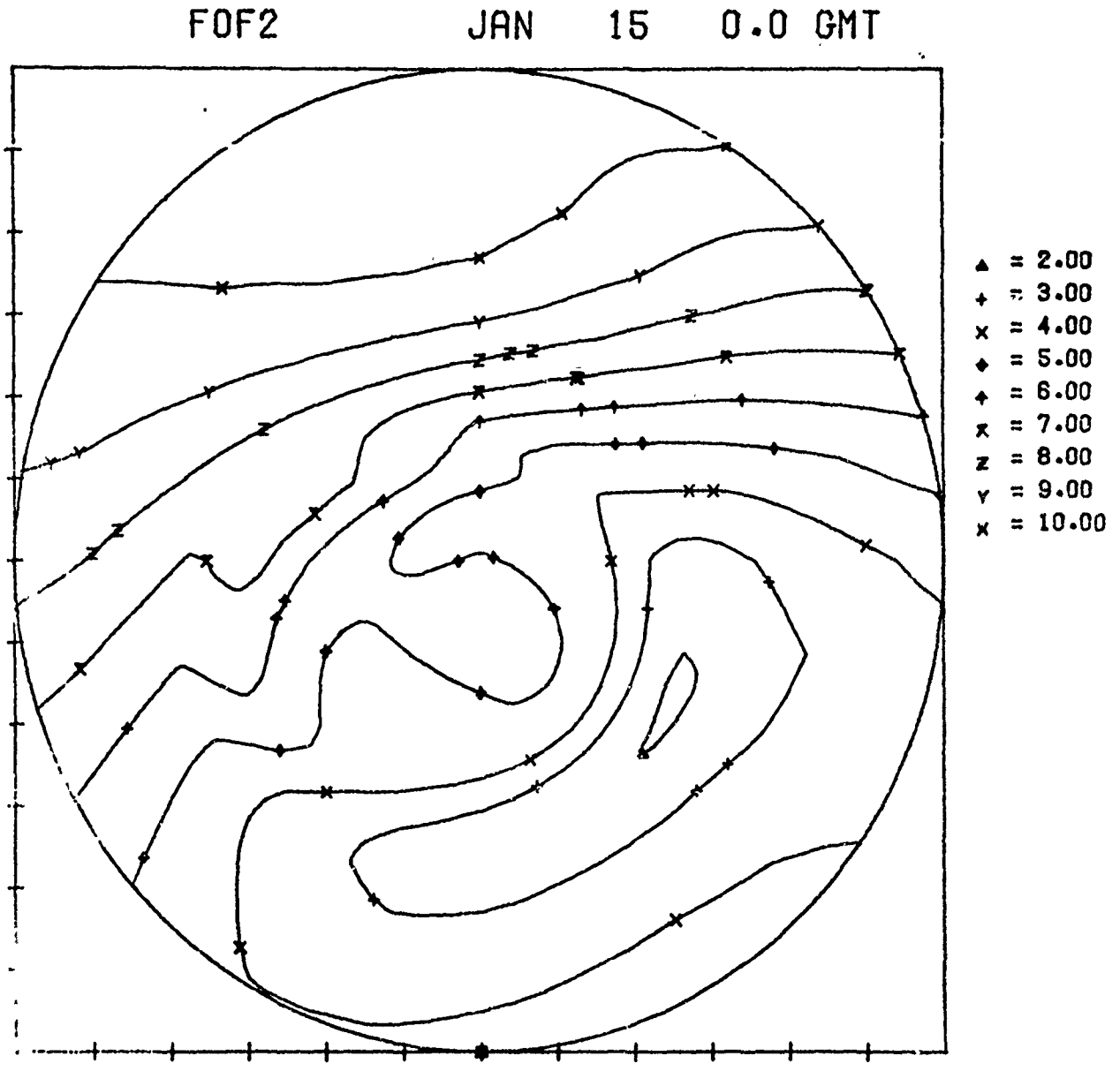


GEOGRAPHIC COORDINATES

Figure II-8

## REFERENCES


(1) Elkins, T. J. (1973) An Empirical Model of the Polar Ionosphere, Air Force Surveys in Geophysics, No. 267, AFCRL-TR-0331.

(2) Jones, W. B., and Gallet, R. M. (1962) Representation of divinal and geographic variations of ionospheric data by numerical methods, ITU Tellecomm. Jour. 29, 129-149.

(3) Jones, W. B., Leftin, M., Obitts, D. L., (1973) Improved Numerical Representation of Ionospheric Characteristics at High Latitudes, ITS unpublished.

## III. IMPROVEMENTS IN RAY TRACING TECHNIQUES

### A Three Dimensional Ray Tracing Computer Program (ARCON II)

In the past year, we have continued our work in the development of improved ray tracing techniques. This work encompassed several major modifications to the ARCON Version I three dimensional ray tracing program. [1], [2], [3] These changes allowed for greater versatility, faster execution times, more efficient computer core allocation, reduction in programming required by the user and the consolidation of alternative subprograms implementing various user options.

The following pages describe the subprograms in which substantive changes were made to ARCON Version I. No substantive changes were made to the subroutines: TRACE, HASEL, RKAM, BACKUP, REACH and POLCAR. The job setup is described in TABLE III-1. Details of the input file are described in TABLE III-2 and the details of the ionospheric specification file are described in TABLE III-3.

## A. SUBROUTINE RAYTRC

RAYTRC is the main subroutine for the ARCON ray tracing program. It calls the initialization routine READW, and organizes calls to the ray tracing subroutine RANGER in one of three sequencing modes. These modes are "scatter," "homing," and "skip distance" sequencing which are respectively selected by a "1", "2" or "3" punch in column 30 of the option card described in the INPUT file description.

"Scatter" sequencing is the original sequencing mode. Loops are constructed to step by equal intervals through ranges in elevation, azimuth, and frequency. Certain modifications were implemented to allow for desired options in particular applications. First, the scan in elevation angles is terminated as soon as a ray in the set has penetrated the ionosphere. This feature may be turned off by specifying a negative elevation step in the W array, or by punching character "1" in column 80 of the option card. Second, should the azimuth step be zero subsequent rays in the elevation scan are corrected for azimuthal deviation to attempt closer down range landing at a given azimuth. This feature may be turned off by punching character "1" in column 75 of the option card, or by specifying a non zero azimuth step. Third, an algorithm to compute the backscatter amplitude at each frequency was included. This calculation is not accomplished unless at least two elevations and two azimuths are traced.

"Homing" sequencing implements a linear Newton iteration algorithm in elevation and azimuth to determine the elevation and azimuth at each frequency to illuminate a given down range target. Since the algorithm is linear, it tends to be unstable near the skip distance. For the first frequency, the initial elevation is taken from the W array (element 255) and the initial azimuth is taken as the azimuth to the target. The user should take care to specify the initial elevation less than the skip distance elevation and, if F mode transmission is desired, greater than the E to F mode switching elevation. The initial elevation for the second frequency is taken

as the solution elevation for the first frequency. For subsequent frequencies, the initial elevations are extrapolated from the solutions for the previous two frequencies. The initial azimuths for the second and subsequent frequencies are taken as the solutions for the last frequencies. The user specifies the geographic latitude and east longitude as elements (11) and (12), respectively, of the W-array. The program computes the required range and azimuth. Analysis of the homing algorithm implemented, and discussion of its application in various ionospheres is contained in Section IV of this report.

"Skip Distance" sequencing quickly locates the skip distances for the sequence of frequencies at a single azimuth. Elevations are scanned backward from the final elevation (W(256)) toward the initial elevation (W(255)) in $1^{o}$ steps until the ionosphere ceases to be penetrated; thereafter, the elevation scan continues towards lower elevations in $1/2^{o}$ steps until the ground range begins to increase. The elevation is incremented by the elevation step (W(257)) the frequency is incremented by the frequency step (W(260)) and the process is repeated until either the frequency loop is completed or an elevation angle less than the initial elevation (W(255)) is encountered.

## B. SUBROUTINE READW

Initialization features originally scattered among several different subroutines were collected together in the INPUT file processing routine READW. This program initializes labelled common blocks with data statements, clears the INPUT file of the next run identification card, optio, card, and W array cards. Non zero elements of the W array are listed, and elements of the W array are distributed to other labelled common blocks. The orthogonal transformation matrices among geographic, dipole, and transmitter coordinate systems are computed via calls to XFRM. The coordinates of each pole and receiver in each system are listed. Elements of the option list are checked to construct a message, listed later, describing the options for that run. A call to FILEIN initializes the ionosphere. The time required for initialization tasks is computed and written to the output file.

## C. COMPLEX FUNCTION XFRM (X, R)

This is a general application subprogram to compute the orthogonal transformation matrix between various coordinate systems. Alternate entry points GTOD and DTOG compute the transformed spherical coordinates.

The argument R (nine element array) is the orthogonal transformation matrix, while X (declared complex) contains colatitude and east longitude in the real and imaginary parts respectively. Similarly, the function return contains colatitude and east longitude.

Entry point XFRM computes the transformation matrix R to a coordinate system with pole through point X in the old system. The prime meridian of the new system is the great circle containing both poles. The function return is the new pole X.

Entry point GTOD returns the coordinates in the new system corresponding to coordinates X in the old, while DTOG returns old system coordinates corresponding to new system coordinates X.

## D. SUBROUTINE FILEIN (N, M, PFA)

FILEIN processes the ionosphere file described in Table III-1. The arguments specify which subfile to read from, how many records to list, and where to store the plasma frequency array:

| | |
|---|---|
| N < O | Rewind file, position to $(-N)^{th}$ subfile. |
| N > O | No rewind, position to $N^{th}$ subfile. |
| N = O | No file action, continue with current ionosphere. |
| M < O | Single profile option. Read and list $(-M)^{th}$ profile, skip to end of subfile, set up ionosphere domains to reflect universal spherically symmetric ionosphere. |
| M ≥ O | Read entire file, list first M+1 profiles. |
| PFA | First word address of plasma frequency array. |

The routine first positions the ionosphere file to the desired subfile, and reads the ionosphere parameter record. The upper and lower limits of the domain of the ionosphere in kilometers of altitude, degrees of latitude, and degrees of longitude are computed and stored in the first six elements of common block/CRDLMTS/. The ionosphere parameters are printed. The core required to store the array is computed and a call to NRFL establishes the field length at the required element of PFA. The ionosphere is then read in profile by profile, and listed as requested.

Note that FILEIN does not require positive definite grid spacings, a feature which removes constraints on the user previously imposed.

Note also that the user is relieved of the burden to allocate core memory; function NRFL (described below) dynamically increases or decreases field length to reflect requirements.

## E. FUNCTION NRFL(A)

This is a FORTRAN callable CDC6600 COMPASS subprogram that allows the user to increase or decrease core memory allocated to the job at any time during execution, subject, of course, to the maximum core limit specified on the job card.

The argument A must be a simple variable name or array element in blank common. The subprogram establishes the field length of the job at the address defined by the argument, writes a message to the dayfile, FL-nnnnnn, where nnnnnn is the address defined by A, and returns via the function call the address of A.

## F. SUBROUTINE PRINTR (NWHY)

Changes resulting in substantial core memory savings were implemented in the basic output routine. These consisted primarily in removing the initialization features to the initialization subprogram. The output line format, however, was not changed. The argument NWHY still remains as a display code menomic indicating the ray states triggering the call to PRINTR. Each output line contains the following information:

| Item | Format | Description |
|---|---|---|
| 1 | IXE8.1 | relative error in group speed squared |
| 2 | IXA8 | NWHY |
| 3 | F8.2 | altitude in kilometers |
| 4 | F9.2 | ground range in kilometers |
| 5 | F7.2 | angle in degrees between ray and field |
| 6 | F7.2 | magnetic colatitude |
| 7 | F7.2 | magnetic east longitude |
| 8 | F7.2 | azimuthal deviation |
| 9 | F7.2 | local azimuthal deviation |
| 10 | F7.2 | elevation of field point from transmitter |
| 11 | F7.2 | local elevation of ray path |
| 12 | F7.2 | real part of polarization |
| 13 | F7.2 | imaginary part of polarization |
| 14 | F8.2 | group path length |
| 15 | F8.2 | phase path length |

The first call to PRINTR for each ray traced will print column headings. PRINTR will recompute the magnetic field for purposes of computing item 5 if the output magnetic field (field 7 of the option card) specifies a more accurate magnetic field than included in the refractive index calculation.

## G. FUNCTION RANGER (FREQ, EL, AZ)

This function subprogram was inserted as a buffer between the ray selection routine RAYTRACE and the ray tracing routine TRACE. The three arguments are, respectively, ray frequency in megahertz, takeoff elevation in radians, and takeoff azimuth in radians. The function return is the ground range in kilometers (taken from the PRINTR output list) upon return from subroutine TRACE.

The program performs some initialization for each ray traced. It writes one line on the output file specifying the frequency in megahertz, azimuth in degrees, and elevation in degrees. It computes the initial conditions for the ray, and aborts if the ray is in an evanescent region. It calls in the fundamental ray tracing routine TRACE, and prints the time required to execute each ray.

## H. SUBROUTINE ELECTX

This subroutine computes the parameter X and its derivatives, where X is the squared ratio of ionosphere plasma frequency to working frequency.

The plasma frequency and its derivatives are computed by calling a general second order interpolation algorithm in three variables, FOXYZ. Initialization of the common blocks required, and input of the plasma frequency array is accomplished in SUBROUTINE FILEIN.

The program must convert the field point variables from geocentric distance in kilometers to altitude in kilometers, colatitude in radians to latitude in degrees, and east longitude in radians to east longitude in degrees. Furthermore, an initial domain check of longitude is necessary, adding or subtracting $360^{\circ}$ if out of range, before calling FOXYZ. This removes from the user the burden of unnecessary rigor of selecting longitude branch domain.

Should the user desire to use an analytic electron density model, he need only replace this routine and SUBROUTINE FILEIN (N1, N2, PFA). The user may use the latter routine for initialization purposes; it is called once for each W-array specified on the INPUT file.

## I. FUNCTION FOXYZ(X, Y, Z, F, IX, IY, IZ)

FOXYZ implements a general second order interpolation algorithm within a tabulated function of three variables. The elements of the argument list are:

| | | |
|---|---|---|
| X, Y, Z | - | coordinates of the field point at which the interpolated value of the function is desired |
| F | - | first word address of tabulated array of function values |
| IX, IY, IZ | - | array dimensions |

The function return is the interpolated function value.

Prior to calling this routine, elements of certain labelled common blocks, /CRDLMTS/and/IONOSPH/, must be defined in addition to filling in the array F. These elements are listed below:

/CRDLMTS/XMIN(3), XMAX(3), MINMAX(3), IFLG, LN(2)
/IONOSPH/NAME, LN(3), XO(3), DX(3), DM(5)

| | |
|---|---|
| XMIN | lower limits of function definition |
| XMAX | upper limits of function definition |
| MINMAX | defined by FOXYZ, see below |
| IFLG | defined by FOXYZ, see below |
| LN | not used |
| NAME | not used |
| LN | array dimensions, must agree with IX, IY, IZ of argument lis |
| XO | coordinates of first element of F |
| DX | uniform grid spacings |
| DM | not used |

In the above arrays, indices 1, 2, 3 correspond respectively to coordinates X, Y, Z; thus, the proper domain of variable X is given by

$$XMIN(1) \leq X \leq XMAX(1).$$

The program first checks the field point variables against their respective proper domains. If any variable is less than its minimum value, the corresponding element of MINMAX is set to -1, if greater than the maximum, MINMAX is set to +1; otherwise, MINMAX is set to zero. If any variable is outside its proper domain, IFLG is set to +1, otherwise, IFLG is set to zero.

If variable X is outside its proper domain, a value of 0 is returned via the function call. However, if Y and/or Z are outside their domains, second order interpolation proceeds only in X, at the nearest profile.

The program stores local variables in labelled common block/SCRATCH/, 64 words in length, certain elements of which may be of interest and use to the user. These elements are listed below.

/SCRATCH/SC(64)

| element | definition on return from FOXYZ |
|---|---|
| 12,13,14 | $\partial F/\partial x$, $\partial F/\partial y$, $\partial F/\partial z$ |
| 15,16,17 | $\partial^2 F/\partial x^2$, $\partial^2 F/\partial y^2$, $\partial^2 F/\partial z^2$ |
| 18,19,20 | $\partial^2 F/\partial y \partial z$, $\partial^2 F/\partial z \partial x$, $\partial^2 F/\partial x \partial y$ |

## J. SUBROUTINE RINDEX

This program was modified to include all cases. The program calls subprograms ELECTX, DIPY, and COLFRZ to compute the electron density, magnetic fields, and electron collision frequencies respectively. Each contribution is value checked, and if zero complicated computations are bypassed to execute simpler algorithms.

Core storage conservation was accomplished by (1) sharing local variable storage with other routines in labelled common block /SCRATCH/, (2) using DO loops for contributions by the magnetic field components, (3) eliminating non essential complex variable calculations, and (4) eliminating the complex attribute from variables of which only the real part is ultimately used. Many of these steps also resulted in reduction of execution time.

## K. FUNCTION DIPY (YEAR, R, THETA, PHI, NORDER)

This subprogram computes a spherical harmonic approximation to the earth's magnetic field. The arguments are:

| | |
|---|---|
| YEAR | - year to which to update the harmonic coefficients |
| R | - geocentric distance in kilometers |
| THETA | - magnetic dipole colatitude in radians |
| PHI | - magnetic dipole east longitude in radians |
| NORDER | - order of approximation from O (no field) to 8 (maximum) |

The function return is the magnetic potential.

The components and their derivatives of the magnetic field are returned via labelled common block/DIPYOUT/, eighteen words in length:

| word | definition |
|---|---|
| 1 | magnetic potential |
| 2 | field magnitude in gammas |
| 3,4,5 | derivatives of field magnitude |
| 6-9 | radial component and derivatives |
| 10-13 | southward component and derivatives |
| 14-17 | eastward component and derivatives |
| 18 | dip angle |

TABLE III-1: JOB SETUP FOR RAYTRACE PROGRAM

```
JOB CARD
ATTACH, TAPE4.  Cards to attach file of ionospheres
ATTACH, MODELX, MODELX3141, ID=GIBBS, MR=1.
LIBRARY, MODELX.
FTN.
LGO.
7/8/9
          PROGRAM MAIN (INPUT, OUTPUT, TAPE4)
          CALL RAYTRC
          END
7/8/9
IDENTIFICATION CARD
OPTION CARD
W ARRAY CARDS
:
BLANK CARD - causes execution
(Repeat as often as desired.  Terminate run with W-array element
negative)
6/7/8/9
```

## TABLE III-2: INPUT FILE EXPECTED BY READ W

| CARD | FORMAT | DESCRIPTION |
|---|---|---|
| 1 | 8A10 | descriptive text to be listed on OUTPUT |
| 2 | 16I5 | option card |
| 3 to N | I3, E14.7, 4I1 | W array cards |
| N+1 | Repeat from card 1 as often as desired | |

### OPTION CARD DESCRIPTION

| FIELD | FUNCTION | USED IN |
|---|---|---|
| 1 | ≠0 produces output to TAPE 1 | PRINTR |
| 2 | = 0 inhibits output to OUTPUT | PRINTR |
| 3 | selects ionosphere from TAPE 4 | FILEIN |
| 4 | selects profiles to list | FILEIN |
| 5 | selects magnetic field option | DIPY & RINDEX |
| 6 | selects sequencing mode | RAYTRC |
| 7 | selects output magnetic field | PRINTR |
| 8 | reserved for collision frequency option | |
| 9-14 | not used | |
| 15 | ≠ 0 inhibits azimuth correction | RAYTRC |
| 16 | = 0 inhibits elevation scan | RAYTRC |

### W ARRAY CARD DESCRIPTION (see reference 2)

| FIELD | VALUE | FUNCTION |
|---|---|---|
| 1 | 1-400 | W array element |
| | 0 | end of W-array, start ray trace |
| | <0, >400 | terminate job |
| 2 | REAL | W array value |
| 3 | ≠0 | Convert value from degrees to radians |
| 4 | ≠0 | Convert value from kilometers to radians |
| 5 | ≠0 | Convert value from nautical miles to kilometers |
| 6 | ≠0 | Convert value from feet to kilometers |

## TABLE III-3: TAPE4-ionosphere file

### STRUCTURE OF IONOSPHERE FILE expected by FILEIN

FILE STRUCTURE

| RECORD | DESCRIPTION | LENGTH |
|---|---|---|
| 1 | IONOSPHERE GRID PARAMETERS (IGP) | 15 |
| | PLASMA FREQUENCY PROFILES (PFP) | L+6 |
| 2 | first latitude, first longitude | |
| M+1 | last latitude, first longitude | |
| M+2 | first latitude, second longitude | |
| M*N+1 | last latitude, last longitude | |
| M*N+2 | EOF (may be absent) | 0 |
| M*N+3 | IGP-second file | 15 |
| | etc. | |

RECORD STRUCTURE

| WORD | | DESCRIPTION | | TYPE | DIMENSION |
|---|---|---|---|---|---|
| IGP | 1 | Name of Ionosphere | | Display Code | - |
| | 2 | Number of altitudes | (L) | integer | - |
| | 3 | Number of latitudes | (M) | integer | - |
| | 4 | Number of longitudes | (N) | integer | - |
| | 5 | First altitude | (HO) | real | kilometers |
| | 6 | First latitude | | real | degrees |
| | 7 | First longitude | | real | degrees |
| | 8 | altitude step | (DH) | real | kilometers |
| | 9 | latitude step | | real | degrees |
| | 10 | longitude step | | real | degrees |
| | 11 | Date Time Group | | Display Code | - |
| | 12 | F10.7 | | real | |
| | 13 | SUNSPOT number | | real | |
| | 14 | AP | | real | |
| | 15 | KP | | real | |
| PFP | 1 | Profile length | (L) | integer | - |
| | 2 | First altitude | (HO) | real | kilometers |
| | 3 | Profile latitude | | real | degrees |
| | 4 | Profile longitude | | real | degrees |
| | 5 | last altitude | (HM) | real | kilometers |
| | 6 | altitude step | (DH) | real | kilometers |
| | 7 | Plasma Frequency at HO | | real | MHZ |
| | L+6 | Plasma Frequency at HM | | real | MHZ |

## References


(1) Friedman, M., Miller, D. C., Vanguri, K. S. etal. (1973) Mathematical and Statistical Analysis for the Reduction of Ionospheric Data. AFCRL-TR-73-0698.

(2) Jones, R. M., and Stephenson, J. J. (1970) A Three Dimensional Ray Tracing Computer Program (unpublished).

(3) A Three Dimensional Ray Tracing Computer Program (1973) ARCON I prepared for AFCRL (unpublished).

## IV. ANALYSIS OF A HOMING TECHNIQUE IN THREE DIMENSIONAL IONOSPHERIC RAY TRACING

### A. Development of Homing Algorithm

We desire to determine the takeoff elevation and azimuth of a ray illuminating a given target from a given transmitter at a given frequency. Let the position of the target be specified by the range $R_T$ and azimuth $A_T$ from the transmitter. The relevant results from a ray trace at elevation E and azimuth A are the range R(E, A) and downrange azimuth $A_R$ (E, A). The homing solution, $E_H$ and $A_H$, is found by inverting the equations,

$$\begin{aligned} R\ (E_H,\ A_H) &= R_T, \\ A_R\ (E_H,\ A_H) &= A_T. \end{aligned} \tag{1}$$

In the neighborhood of $E_0$, $A_0$, R (E, A) and $A_R$ (E, A) may be approximated by

$$\begin{aligned} R\ (E,A) &= R_0 + R_E\ (E-E_0) + R_A\ (A-A_0) \\ A_R\ (E,A) &= A_{R0} + A_E\ (E-E_0) + A_A\ (A-A_0) \end{aligned} \tag{2}$$

where $R_0 = R\ (E_0,\ A_0)$, $A_{R0} = A_R(E_0, A_0)$, $R_E$ and $R_A$ are the derivatives of R at $E_0$, $A_0$, and $A_E$, $A_A$ are the derivatives of $A_R$.

Thus the inversion of equations reduces to solving for $E_H$ and $A_H$ the linear simultaneous equations,

$$R_E\,(E_H - E_0) + R_A\,(A_H - A_0) = R_T - R_0 = \Delta R$$
$$A_E\,(E_H - E_0) + A_A\,(A_H - A_0) = A_T - A_{R0} = \Delta A_R \qquad (4)$$

Thus,

$$E_H + E_0 + \Delta E,$$
$$A_H = A_0 + \Delta A, \qquad (5)$$

where,

$$\Delta E = (\Delta R \cdot A_A - \Delta A_R \cdot R_A) \,/\, (R_E \cdot A_A - A_E \cdot R_A)$$
$$\Delta A = (\Delta A_R \cdot R_E - \Delta R \cdot A_E) \,/\, (R_E \cdot A_A - A_E \cdot R_A)\,. \qquad (6)$$

Starting from E , A as a good first approximation, iteration of equations (4) converges rapidly to the solution.

In principle, computation of the derivatives appearing in equations (5) requires tracing three rays at each iteration. However, considerable simplification is possible.

The ranges of a family of ray tracings are primarily dependent on elevation and relatively insensitive to azimuth changes. Furthermore, the downrange azimuthal deviation $\delta$ is slowly varying and relatively insensitive to changes in initial conditions. Thus, we may set $A_E = R_A = 0$, and $A_A = 1$; equations (2) simplify to,

$$R\,(E,\ A) = R_0 + R_E\,(E - E_0)$$
$$A\,(E,\ A) = A - \delta \qquad (7)$$

Equations (4) for successive approximations to the homing solution reduce to,

$$E_H = E_0 + (R_T - R_0) / R_E$$
$$A_H = A_T + \delta \tag{8}$$

The remaining derivative of R is given by the finite difference formula,

$$R_E = \left(R(E_1) - R(E_2)\right) / (E_1 - E_2) \tag{9}$$

The final algorithm implemented in the homing mode of ray tracing generates a sequence of elevations and azimuths $E^{(n)}$, $A^{(n)}$ given by

$$\begin{aligned} E^{(0)} &= E_0 \\ E^{(1)} &= E^{(0)} + \Delta E_0 \\ E^{(n+1)} &= E^{(n)} + \left(E^{(n)} - E^{(n-1)}\right) \cdot \left(R_T - R^{(n)}\right) / \left(R^{(n)} - R^{(n-1)}\right) \\ A^{(0)} &= A_T \\ A^{(n+1)} &= A_T + \delta^{(n)} \end{aligned} \tag{10}$$

where $E_0$ and $\Delta E_0$ are specified by the user, $R^{(n)}$ and $\delta^{(n)}$ are the range and azimuthal deviation of the nth iteration. The user specifies geographic latitude and east longitude of the target receiver from which the program computes $A_T$ and $R_T$.

Iteration of equations (10) terminates when the range error $|R_T - R^{(n)}|$ is less than one kilometer or when n = 10.

B. Ray Tracing in Rush-Miller Ionospheres

The Rush-Miller Electron Density Model with ITS model foF2 and HmF2 was used to generate ionospheres of plasma frequency profiles over the domain $36^{\circ}$ N to $4^{\circ}$ N magnetic and $14^{\circ}$ W to $55^{\circ}$ E magnetic. The solar cycle was taken at mean conditions (solar flux 100 and sun spot number 50), and equinox (March 21) ionospheres were constructed for $0^{h}$ and $6^{h}$ Eastern Standard Time. These two ionospheres will be referred to as the Midnight and Sunrise ionospheres hereafter.

We traced rays in both ionospheres from a transmitter located at $24.5^{\circ}$N and $81.5^{\circ}$W geographic at an azimuth of $108^{\circ}$ True and a frequency of 6 MHZ. This frequency is about 20% larger than the mean F2 critical frequency along the path. We used a null magnetic field, and integrated the ray tracing equations with 8 kilometer steps.

Figure IV-1 displays plasma frequency profiles for several ranges along azimuth $108^{\circ}$ True for the sunrise ionosphere, and shows the development of the ionospheric E layer from shorthy before to about an half hour after sunrise.

Figure IV-2 is a presentation of several ray traces across the sunrise line. The altitude scale is four times larger than the range scale. These are crude ray traces in that only the critical points are plotted (enter and exit ionosphere, reflection and ground return) connected by straight lines.

Figure IV-3 is a range versus elevation presentation of ray traces in the midnight and sunrise ionospheres.

Even though the sunrise line is positioned from the transmitter to present the most difficulty, figures IV-2 and IV-3 reflect considerable regularity. Note from figure IV-2 that the switch over from E to F mode transmission ($3^{\circ}$ to $4^{\circ}$) occurs while the rays are entering the ionosphere on the sunlit side.

The major anomaly in ray tracing across the sunrise line occurs for rays ($14^{\circ}$ to $17^{\circ}$) entering the ionosphere near the high altitude knee of the

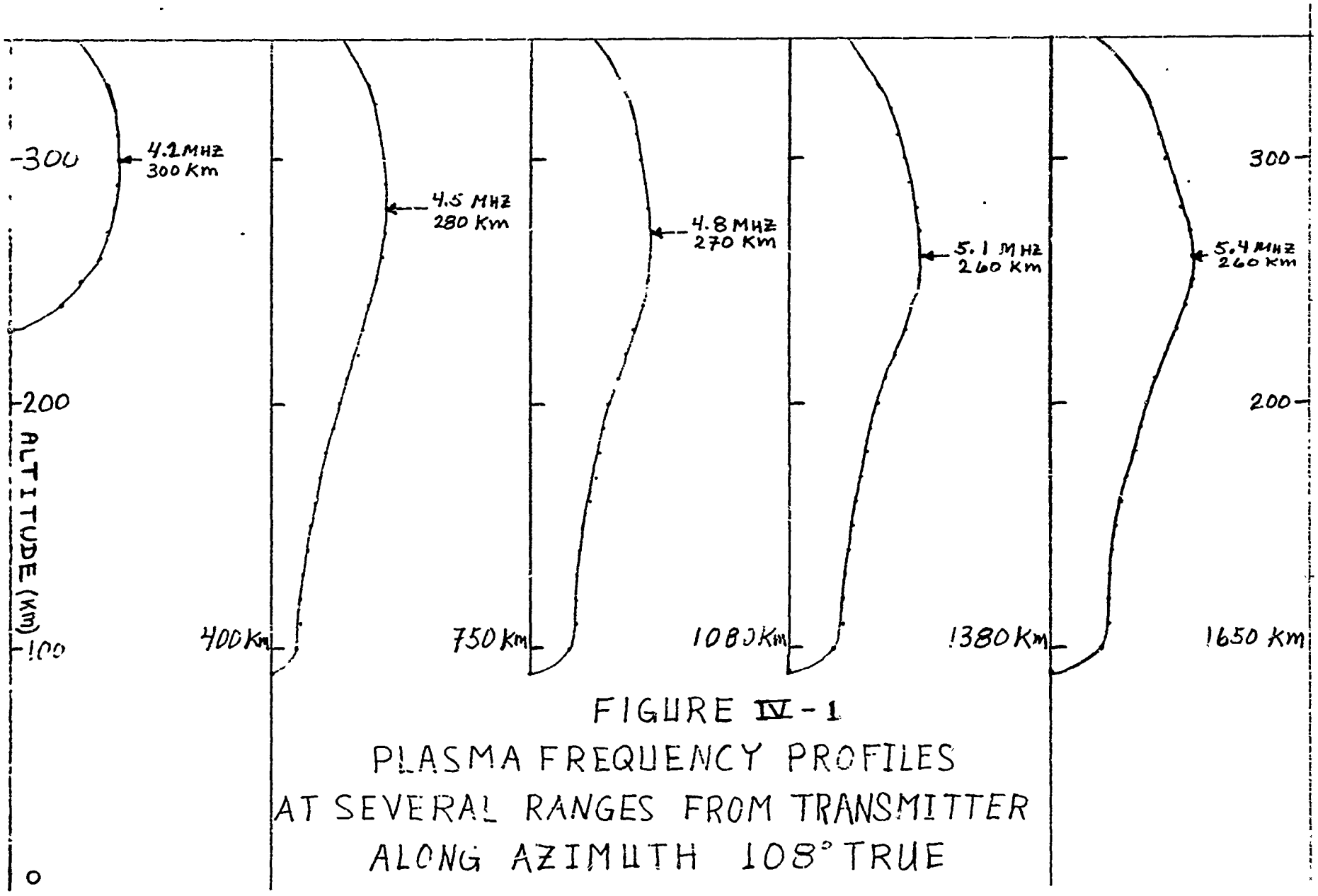


FIGURE IV-1

PLASMA FREQUENCY PROFILES

AT SEVERAL RANGES FROM TRANSMITTER

ALONG AZIMUTH 108° TRUE

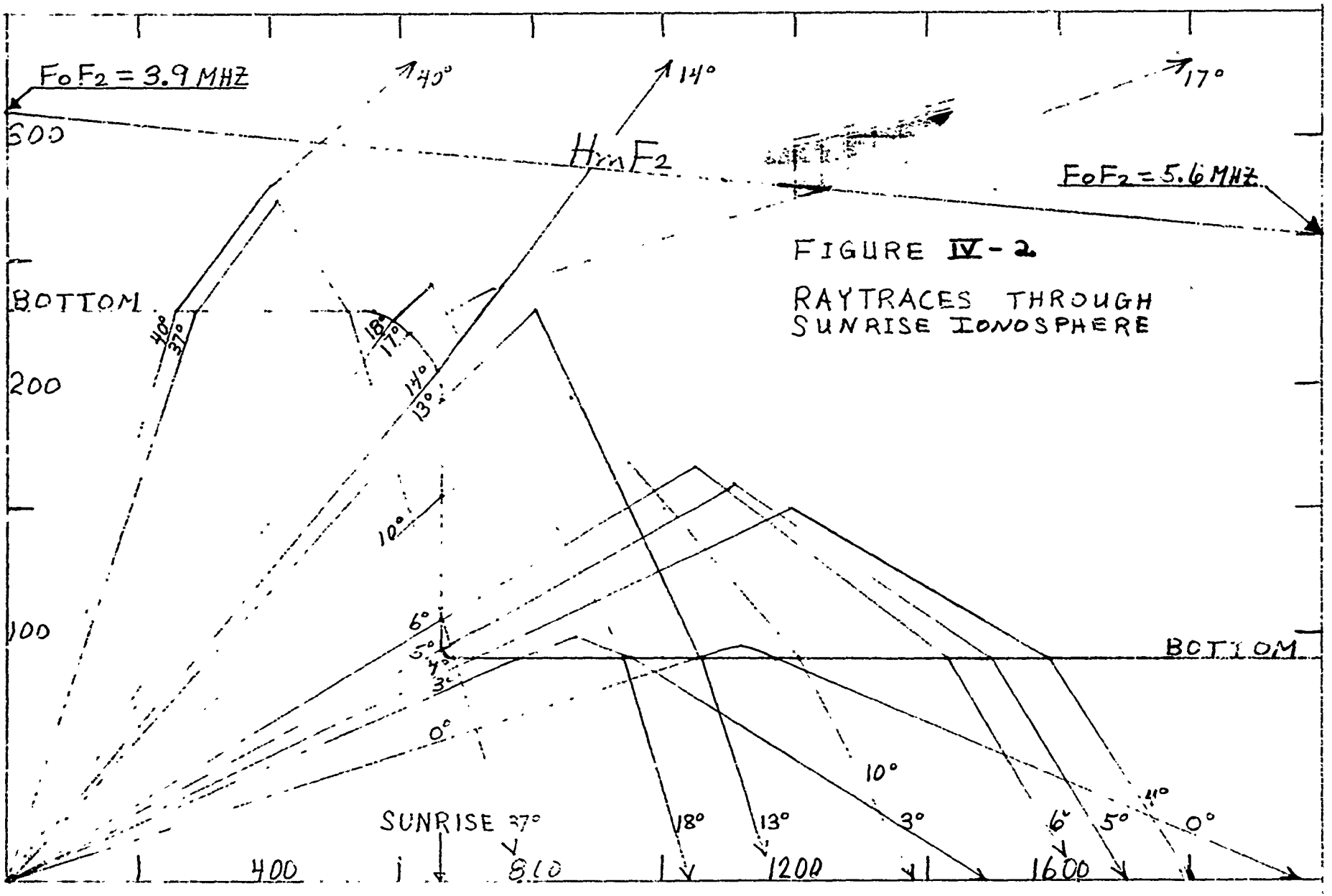


FIGURE IV-2

RAYTRACES THROUGH SUNRISE IONOSPHERE

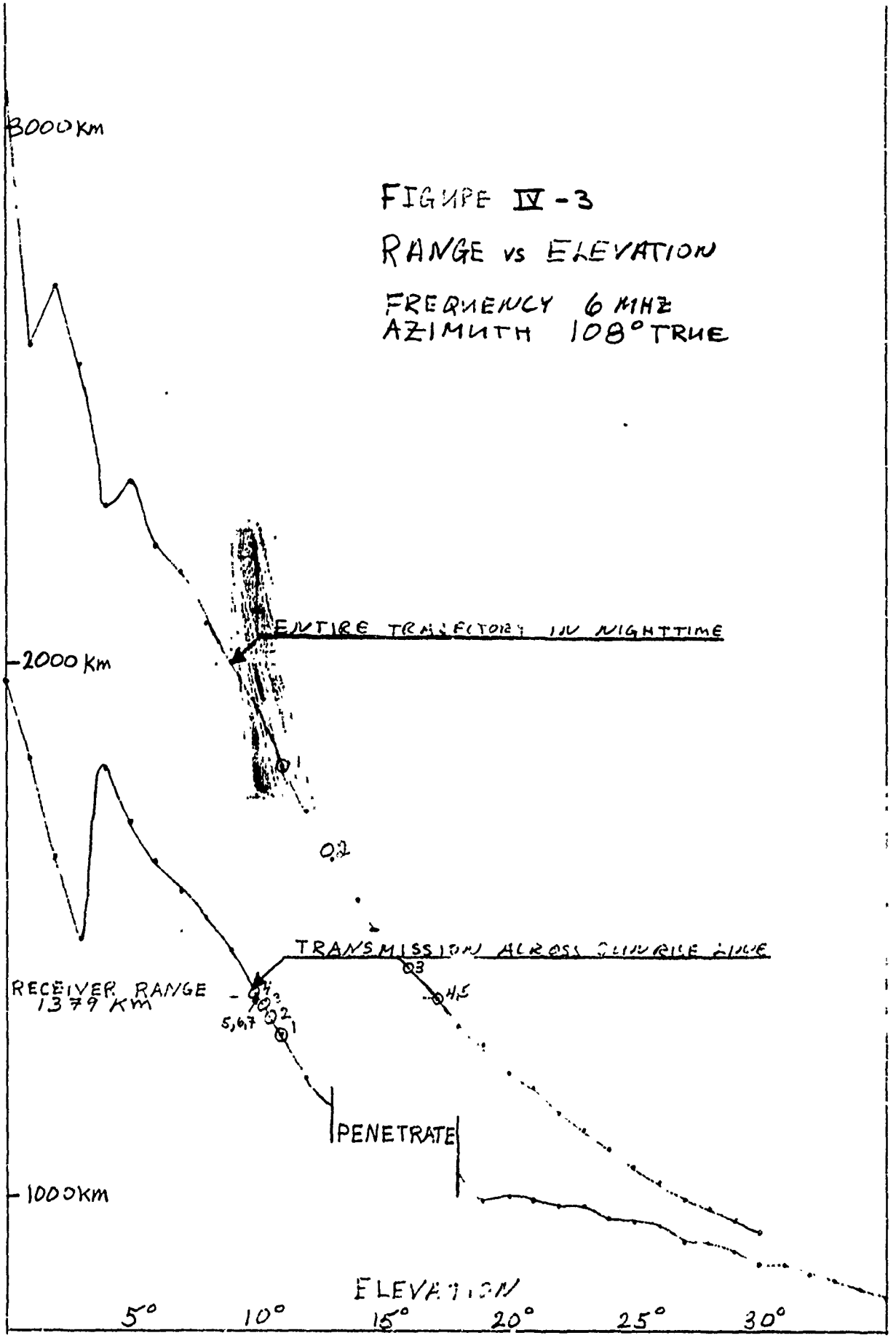
FIGURE IV-3
RANGE vs ELEVATION
FREQUENCY 6 MHZ
AZIMUTH 108° TRUE
3000 Km
2000 Km
1000 Km
ENTIRE TRANSMISSION IN NIGHTTIME
TRANSMISSION ACROSS TERMINATOR LINE
RECEIVER RANGE 1379 Km
PENETRATE
ELEVATION
5°
10°
15°
20°
25°
30°

FIGURE IV-4

RANGE VS. ELEVATION
TRANSMISSION ALONG SUNRISE LINE
FREQUENCY 6 MHZ

X = GRAZING APPROACH TO EARTH

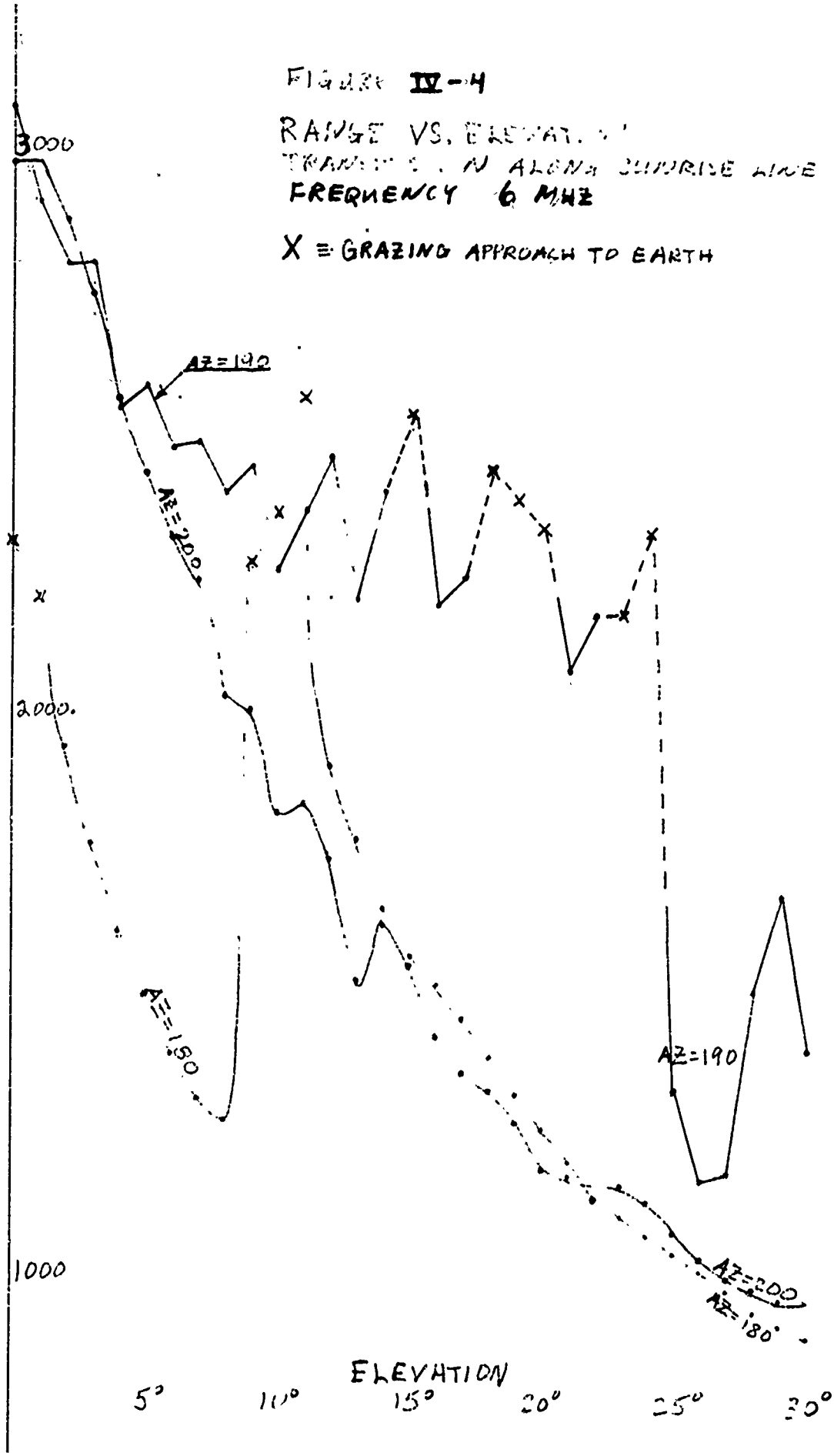

ionosphere bottom. The high horizontal gradients at this point tend to turn the ray upwards, and effectively create a hole in the ionosphere through which the rays penetrate into space. This anomaly, of course, reflects the structure of the Rush-Miller ionospheric model which may or may not be a fully adequate representation of the actual conditions that prevail near sunrise and sunset.

Although the ray trace program appears to be reliable for tracing rays across the sunrise line, severe difficulties associated with extreme transverse gradients are encountered when tracing rays along the sunrise. Figure IV-4 represents range elevation curves from a transmitter located $1^{\circ}$ east of sunrise transmitting close to the sunrise line.

At azimuth $180^{\circ}$ True transmission is entirely in the daylight side. The range elevation curve is relatively smooth. Rays are deflected westward by $3^{\circ}$ to $4^{\circ}$ in F-mode transmission.

At azimuth $200^{\circ}$ True, transmission is entirely in the night ionosphere up to $11^{\circ}$ elevation. Beyond $11^{\circ}$ the ray enters the day ionosphere, exits the ionosphere across the sunrise surface and reenters the night ionosphere. The range elevation curve (Figure IV-4) is close to that at $180^{\circ}$ demonstrating the dominance of the F2 layer in determining transmission in F mode.

At azimuth $190^{\circ}$ True, transmission is along the sunrise surface. Figure IV-4 shows that the ray tracing program does not yield stable results. No improvement in smoothing this curve resulted on reducing the integration step size from 8 kilometers to 1 kilometer. Clearly, this instability would preclude meaningful results in an attempt to compute a homing solution.

C. Homing in Rush-Miller Ionospheres

The homing mode of the ray trace program was used to compute homing solutions from a transmitter at $24.5^{\circ}$N, $81.5^{\circ}$W geographic to a target receiver at $20.0^{\circ}$N, $69.0^{\circ}$W geographic at a frequency of 6 MHZ. This

corresponds to a ground range of 1379 km at an azimuth of 108.8° True. The initial elevation was selected from the range elevation curves of figure IV-3.

The results of successive rays in approaching the solution are tabulated in tables IV-1 and IV-2 for homing in the midnight and sunrise ionospheres respectively. The appropriate points are also plotted on the range elevation curves of figure IV-3.

In the midnight ionosphere convergence to the homing solution was rapid. The transverse gradients in the ionosphere are small resulting in less than 4 kilometers in azimuthal deviation at the neighborhood of the target.

Homing across the sunrise surface tended to converge more slowly the down range azimuthal deviations corresponded to corrections at the target of about 20 kilometers reflecting the higher transverse gradients in the ionosphere.

As expected, an attempt to home nearly parallel to the sunrise surface was unsuccessful due to the instability of the range elevation curve.

TABLE IV-1: HOMING IN MIDNIGHT IONOSPHERE

Frequency: 6 MHZ
Receiver Range: 1379 Km

No magnetic field
Azimuth: 108.8°True

| Ray Nr | Takeoff Azimuth (deg) | Takeoff Elevation (deg) | Azimuthal Deviation (deg) | Range Error (Km) |
|---|---|---|---|---|
| 1 | 108.80 | 11.00 | +0.12 | -426.93 |
| 2 | 108.91 | 12.96 | +0.13 | -266.27 |
| 3 | 108.93 | 16.20 | +0.12 | -51.87 |
| 4 | 108.92 | 16.98 | +0.20 | +3.60 |
| 5 | 109.00 | 16.93 | +0.20 | -0.75 |

TABLE IV-2: HOMING ACROSS SUNRISE SURFACE

Frequency: 6 MHZ
Receiver Range: 1379 Km

No magnetic field
Azimuth: 108.8° True

| Ray Nr | Takeoff Azimuth (deg) | Takeoff Elevation (deg) | Azimuthal Deviation (deg) | Range Error (Km) |
|---|---|---|---|---|
| 1 | 108.80 | 11.00 | -1.23 | +98.14 |
| 2 | 107.57 | 10.55 | -0.96 | +37.01 |
| 3 | 107.84 | 10.28 | -0.96 | +21.44 |
| 4 | 107.84 | 9.90 | -0.86 | -8.74 |
| 5 | 107.93 | 10.01 | -0.91 | +1.62 |
| 6 | 107.89 | 10.00 | -0.88 | -3.36 |
| 7 | 107.92 | 10.01 | -0.89 | +0.70 |